A.H. Mohazzab, L. Dozio
A Spectral Collocation Solution for In-Plane Eigenvalue Analysis of Skew Plates
International Journal of Mechanical Sciences, Vol. 94-95, 2015, p. 199-210
doi:10.1016/j.ijmecsci.2015.03.008

The final publication is available at https://doi.org/10.1016/j.ijmecsci.2015.03.008

A spectral collocation solution for in-plane eigenvalue analysis of skew plates

Amir Hossein Mohazzab[a], Lorenzo Dozio[a,*]

[a]*Department of Aerospace Science and Technology, Politecnico di Milano, via La Masa, 34, 20156, Milano, Italy*

Abstract

Free in-plane vibration analysis of isotropic plates with skew geometry is carried out using the spectral collocation method. The mathematical formulation of the discretized spectral solution is expressed in a concise matrix form which can be directly and easily coded in modern mathematical software packages. A rather comprehensive set of plate cases with various skew angles, aspect ratios, and boundary conditions is presented, with the aim of both showing the rate of convergence and degree of accuracy of the adopted method and providing useful design guidelines related to the effect of the plate geometrical parameters on the fundamental in-plane frequency value.

Keywords: In-plane free vibration, Skew plates, Spectral collocation method, Eigenvalues

1. Introduction

Accurate computation of the in-plane modal characteristics of plates can be of utmost importance in some engineering applications such as transmission of high frequency vibration through a built-up structure [1, 2] or excitation of thin plates subjected to high speed tangential flows.

Owing to the practical interest of the problem, some researchers investigated the in-plane vibration of plates according to different mathematical approaches. About two decades ago, Bardell *et al.* [3] used the Ritz method to study the in-plane frequencies and mode shapes of isotropic rectangular plates with various boundary conditions. The same method was adopted later by others to study the effect of ply orientation in orthotropic and laminated plates [4, 5], the influence of nonuniform elastically restrained boundaries [6] and the modal properties when the plate has non-rectangular geometry [7]. Gorman [8, 9, 10] applied the superposition method to accurately predict the in-plane frequencies of rectangular plates with fully free and clamped edges and uniform elastic supports normal to the boundary. The Kantorovich-Krylov method was employed by Wang and Wereley [11] to compute free in-plane vibration characteristics of rectangular isotropic plates with various combinations of clamped and free edges. Finally, a series solution is obtained

*Corresponding author
Email addresses: ah_mohazzab@yahoo.com (Amir Hossein Mohazzab), lorenzo.dozio@polimi.it (Lorenzo Dozio)

in Refs. [12, 13, 14] for the in-plane vibration analysis of isotropic and orthotropic plates with elastically restrained boundaries.

Besides the aforementioned approximate analytical-type and numerical studies, some exact solutions of the free in-plane vibrations of rectangular plates are also available in the open literature. Gorman [15] analyzed plates having at least two opposite edges simply supported and the other edges free or clamped. In Gorman's work, two distinct types of simple support boundary conditions are formulated: so called simple support type 1 (SS1), where the normal stress and tangential displacement along the edge are zeros, and simple support type 2 (SS2), where normal displacement and tangential stress are zeros. Xing and Liu's work [16] is another significant contribution in this field. They employed the separation of variables method to obtain exact solutions of natural frequencies and mode shapes when at least two opposite edges had either types of simple support conditions previously introduced. All possible exact solutions were successfully obtained, including cases which were not available before. An extension of the same exact procedure to orthotropic plates is presented in Ref. [17].

Despite the availability of the works cited above, the amount of research devoted to free in-plane vibration of plates is still extremely small in comparison to that devoted to free transverse vibration of plates. In particular, very little attention has been given to in-plane vibration analysis of non-rectangular plates with straight edges. To the best author's knowledge, the topic is discussed only in the work by Singh *et al.* [7], where a modified form of the Rayleigh-Ritz method is adopted to study rhombic plates. Only few cases with clamped and free edges are numerically investigated in Ref. [7]. Skew plates are of practical interest in the aerospace industry due to the increasing use of such components in aircraft and space vehicles. Indeed, there are extensive studies on the transverse vibration of plates with skew geometry (see, for instance, [18] and [19] and references therein). The same cannot be said for the in-plane vibration problem. The main purpose of the present paper is to contribute to the literature on vibration of skew plates by providing complete sets of vibration data related to in-plane modal properties of plates with various boundary conditions, different aspect ratios and small and large skew angles.

Since exact solutions cannot be obtained for the problem under study, a numerical approach must be employed. Instead of using a classical finite element method (FEM), the solution of the free in-plane vibration of skew plates is obtained here by a spectral collocation method. The reason is twofold. First, FEM typically requires both huge computational resource to accurately capture high frequency modal behaviour and remeshing for any variation of geometrical parameters. Furthermore, the usual slow convergence of FEM is even worsened by the stress singularities at the obtuse corners of the skew plate. Therefore, FEM appears to be an unsuitable choice especially when extensive optimisation and parametric analysis is to be performed.

Spectral methods [20] are known to have high rate of convergence and accuracy. There are various kinds of spectral methods, which can be classified according to the selection of basis and weighting functions in

the numerical procedure. The spectral collocation method used here, also known as Chebyshev collocation method or pseudospectral method [21], can be considered to be a global spectral method that performs a collocation process, i.e., weighting functions are delta functions centered at special grid points called collocation points. Since the mathematical formulation is simple and powerful enough to produce approximate solutions close to exact values, this method has been largely adopted with success in solving partial differential equations governing many physical phenomena such as fluid dynamics and wave motion. It was also used for the solution of structural mechanics problems. Lin and Jen [22] used the pseudospectral method for computing the bending response of laminated anisotropic plates. The eigenvalues analysis of Timoshenko beams and axisymmetric Mindlin plates is presented by Lee and Schultz [23]. More recently, Sari and Butcher applied the pseudospectral method to study the effect of damaged boundaries on the free transverse vibration of thin, moderately thick and thick rectangular plates [24, 25, 26]. It is worth mentioning that, as pointed out by Shu [27], the pseudospectral method is identical to the differential quadrature method (DQM) [28] when the grid points of DQM are chosen to be the Chebyshev collocation points. It is also noted that, differently from the out-of-plane free vibration problem of thin plates, the application of DQM to in-plane vibration analysis of plates is easier since difficulty in dealing with multiple boundary conditions [29, 30] does not exist.

The paper is organised as follows. Section 2 presents the mathematical formulation in terms of equations of motion and boundary conditions of the problem under study, and the related discretization procedure and eigenvalue problem. The discretization of the boundary-value problem is obtained in a concise matrix form which can be directly and easily coded in modern mathematical software packages. Some numerical results are shown in Section 3. First, the rate of convergence of the method is discussed with respect to FEM solutions and for varying skew angles and boundary conditions. Then, the accuracy of the present approach is evaluated by comparison with some reference cases available in the literature. Finally, the fundamental in-plane frequencies of plates with various aspect ratios, skew angles and boundary conditions are reported. Section 4 contains some concluding remarks.

2. Mathematical formulation

2.1. In-plane equations of motion and boundary conditions

Under the small strains assumption, the in-plane dynamic equilibrium of a homogeneous isotropic plate of thickness h with undeformed midplane Ω (see Figure 1) can be expressed in weak form through the principle of virtual displacements as follows

$$\begin{aligned}&\int_\Omega \left[\delta\frac{\partial u}{\partial x}N_{xx} + \delta\frac{\partial v}{\partial y}N_{yy} + \left(\delta\frac{\partial u}{\partial y} + \delta\frac{\partial v}{\partial x}\right)N_{xy}\right]\mathrm{d}y\mathrm{d}x = \\ &-\int_\Omega \left[\delta u\, m\frac{\partial^2 u}{\partial t^2} + \delta v\, m\frac{\partial^2 v}{\partial t^2}\right]\mathrm{d}y\mathrm{d}x\end{aligned} \tag{1}$$

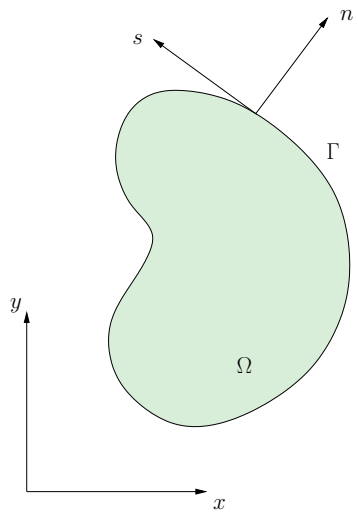

Figure 1: A plate of generic shape Ω and boundary Γ.

where $u = u(x, y, t)$ and $v = v(x, y, t)$ are the displacement components along the in-plane (x, y) cartesian coordinate directions, δ denotes the virtual variation, $m = \rho h$ is the mass per unit area and $N_{\alpha\beta}$ $(\alpha, \beta = x, y)$ are the in-plane stress resultants.

After integrating by parts Eq. (1), the equilibrium can be written as

$$\begin{aligned}
&\int_\Gamma \left[\delta u\, N_{xx} n_x + \delta v\, N_{yy} n_y + \delta u\, N_{xy} n_y + \delta v\, N_{xy} n_x\right] \mathrm{d}s \\
&- \int_\Omega \left[\delta u \frac{\partial N_{xx}}{\partial x} + \delta v \frac{\partial N_{yy}}{\partial y} + \delta u \frac{\partial N_{xy}}{\partial y} + \delta v \frac{\partial N_{xy}}{\partial x}\right] \mathrm{d}y\mathrm{d}x = \\
&- \int_\Omega \left[\delta u\, m \frac{\partial^2 u}{\partial t^2} + \delta v\, m \frac{\partial^2 v}{\partial t^2}\right] \mathrm{d}y\mathrm{d}x
\end{aligned} \tag{2}$$

where Γ is the plate boundary and n_x and n_y are the components of the outward normal $\mathbf{n}$ at a point on Γ. Making use of the constitutive equations and exploiting the arbitrariness of the virtual variations over Ω, the in-plane equations of motion can be written in matrix form as

$$\begin{bmatrix} \mathcal{L}_{11} & \mathcal{L}_{12} \\ \mathcal{L}_{21} & \mathcal{L}_{22} \end{bmatrix} \begin{Bmatrix} u \\ v \end{Bmatrix} = m \frac{\partial^2}{\partial t^2} \begin{Bmatrix} u \\ v \end{Bmatrix} \tag{3}$$

where the elements of the 2×2 matrix of linear differential operators are given by

$$\begin{aligned}
\mathcal{L}_{11} &= A_{11} \frac{\partial^2}{\partial x^2} + A_{66} \frac{\partial^2}{\partial y^2} & \mathcal{L}_{12} &= (A_{12} + A_{66}) \frac{\partial^2}{\partial x \partial y} \\
\mathcal{L}_{21} &= \mathcal{L}_{12} & \mathcal{L}_{22} &= A_{66} \frac{\partial^2}{\partial x^2} + A_{22} \frac{\partial^2}{\partial y^2}
\end{aligned} \tag{4}$$

The quantities A_{ij} are the in-plane rigidities of the plate defined as $A_{11} = Eh/(1 - \nu^2)$, $A_{12} = \nu A_{11}$, $A_{22} = A_{11}$, and $A_{66} = Eh/[2(1 + \nu)]$, where E is Young's modulus and ν is Poisson's ratio.

The boundary integral in Eq. (2) can be alternatively written as

$$\int_\Gamma \left[\delta u_n N_{nn} + \delta u_s N_{ns}\right] \mathrm{d}s \tag{5}$$

where u_n and u_s are the boundary displacements along the normal and tangential directions, respectively, on the boundary Γ (see Figure 1), and N_{nn} and N_{ns} are the corresponding boundary stress resultants. The following relations hold:

$$\begin{aligned}
u_n &= u n_x + v n_y \\
u_s &= -u n_y + v n_x \\
N_{nn} &= N_{xx} n_x^2 + 2 N_{xy} n_x n_y + N_{yy} n_y^2 \\
N_{ns} &= \left(N_{yy} - N_{xx}\right) n_x n_y + N_{xy}\left(n_x^2 - n_y^2\right)
\end{aligned}$$

Therefore, the boundary equations can be expressed in matrix form as

$$\begin{bmatrix} \mathcal{B}_{11} & \mathcal{B}_{12} \\ \mathcal{B}_{21} & \mathcal{B}_{22} \end{bmatrix} \begin{Bmatrix} u \\ v \end{Bmatrix} = \begin{Bmatrix} 0 \\ 0 \end{Bmatrix} \tag{6}$$

where the operators $\mathcal{B}_{ij}$ are defined according to the in-plane boundary conditions. The four classical boundary conditions are here considered: clamped ($u_n = 0$, $u_s = 0$), free ($N_{nn} = 0$, $N_{ns} = 0$), simply-supported type 1 ($u_s = 0$, $N_{nn} = 0$), and simply-supported type 2 ($u_n = 0$, $N_{ns} = 0$). The explicit expressions of $\mathcal{B}_{ij}$ can be found in Appendix A.

2.2. Skew plates in free vibration

From the previous general equations referred to a plate of arbitrary shape, the boundary-value problem of a skew plate can be derived. Let's consider the plate in Figure 2 of side lengths a, b, and skew angle α with respect to the y axis. The boundary-value problem is here expressed in dimensionless form by mapping the (x, y) physical domain Ω into a square (ξ, η) computational domain $\hat{\Omega} = [-1, 1]^2$. The spatial derivatives of any quantity in the two coordinate systems are related by

$$\begin{Bmatrix} \dfrac{\partial}{\partial x} \\[2ex] \dfrac{\partial}{\partial y} \end{Bmatrix} = \begin{bmatrix} \dfrac{2}{a} & 0 \\[2ex] -\dfrac{2}{a}\tan\alpha & \dfrac{2}{b}\dfrac{1}{\cos\alpha} \end{bmatrix} \begin{Bmatrix} \dfrac{\partial}{\partial \xi} \\[2ex] \dfrac{\partial}{\partial \eta} \end{Bmatrix} \tag{7}$$

and

$$\begin{Bmatrix} \dfrac{\partial^2}{\partial x^2} \\[2ex] \dfrac{\partial^2}{\partial y^2} \\[2ex] \dfrac{\partial^2}{\partial x \partial y} \end{Bmatrix} = \begin{bmatrix} \dfrac{4}{a^2} & 0 & 0 \\[2ex] \dfrac{4}{a^2}\tan^2\alpha & \dfrac{4}{b^2}\dfrac{1}{\cos^2\alpha} & -\dfrac{8}{ab}\dfrac{\tan\alpha}{\cos\alpha} \\[2ex] -\dfrac{4}{a^2}\tan\alpha & 0 & \dfrac{4}{ab}\dfrac{1}{\cos\alpha} \end{bmatrix} \begin{Bmatrix} \dfrac{\partial^2}{\partial \xi^2} \\[2ex] \dfrac{\partial^2}{\partial \eta^2} \\[2ex] \dfrac{\partial^2}{\partial \xi \partial \eta} \end{Bmatrix} \tag{8}$$

(a) Physical domain

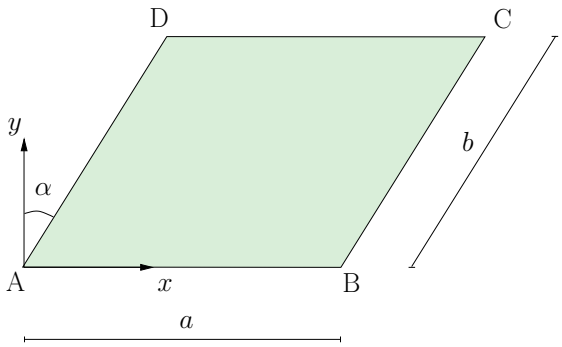

(b) Computational domain

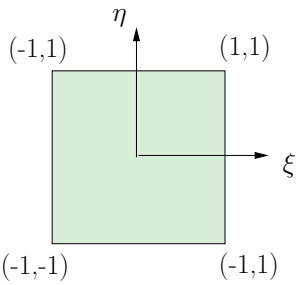

Figure 2: Geometry of the skew plate. (a) Physical domain and (b) computational domain.

After using the above relations into Eq. (4) and assuming a harmonic motion for the in-plane displacements as $(u, v) = (\hat{u}, \hat{v})e^{j\omega t}$, equations (3) can be put into the following ordinary differential eigenvalue form

$$\begin{bmatrix} \hat{\mathcal{L}}_{11} & \hat{\mathcal{L}}_{12} \\ \hat{\mathcal{L}}_{21} & \hat{\mathcal{L}}_{22} \end{bmatrix} \begin{Bmatrix} \hat{u} \\ \hat{v} \end{Bmatrix} = \lambda^2 \begin{Bmatrix} \hat{u} \\ \hat{v} \end{Bmatrix} \tag{9}$$

where

$$\lambda^2 = \frac{\rho a^2 \omega^2 (1-\nu^2)}{4E} \tag{10}$$

and the transformed differential operators are defined as

$$\begin{aligned}
\hat{\mathcal{L}}_{11} &= -\frac{2+(1-\nu)\tan^2\alpha}{2}\frac{\partial^2}{\partial\xi^2} - \frac{1-\nu}{2}\frac{\phi^2}{\cos^2\alpha}\frac{\partial^2}{\partial\eta^2} \\
&\quad + (1-\nu)\phi\frac{\tan\alpha}{\cos\alpha}\frac{\partial^2}{\partial\xi\partial\eta} \\
\hat{\mathcal{L}}_{12} &= -\frac{1+\nu}{2}\left[\phi\frac{1}{\cos\alpha}\frac{\partial^2}{\partial\xi\partial\eta} - \tan\alpha\frac{\partial^2}{\partial\xi^2}\right] \\
\hat{\mathcal{L}}_{21} &= \hat{\mathcal{L}}_{12} \\
\hat{\mathcal{L}}_{22} &= -\frac{2\tan^2\alpha+1-\nu}{2}\frac{\partial^2}{\partial\xi^2} - \frac{\phi^2}{\cos^2\alpha}\frac{\partial^2}{\partial\eta^2} \\
&\quad + 2\phi\frac{\tan\alpha}{\cos\alpha}\frac{\partial^2}{\partial\xi\partial\eta}
\end{aligned} \tag{11}$$

where $\phi = a/b$ is the plate aspect ratio. Accordingly, the related boundary conditions at each edge may be expressed in matrix form as

$$\begin{bmatrix} \hat{\mathcal{B}}_{11} & \hat{\mathcal{B}}_{12} \\ \hat{\mathcal{B}}_{21} & \hat{\mathcal{B}}_{22} \end{bmatrix} \begin{Bmatrix} \hat{u} \\ \hat{v} \end{Bmatrix} = \begin{Bmatrix} 0 \\ 0 \end{Bmatrix} \qquad \text{(each edge)} \tag{12}$$

where, for the sake of brevity, the boundary operators $\hat{\mathcal{B}}_{ij}$ for clamped (C), free (F), simply-supported type 1 (SS1) and simply-supported type 2 (SS2) edges are reported in Appendix B.

2.3. Discretization of the boundary-value problem

A spectral collocation solution of the eigenvalue problem expressed by Eqs. (9) and (12) is derived. Let us first introduce a grid of Chebyshev-Gauss-Lobatto (CGL) points $(\xi_i, \eta_j), i, j = 0, \ldots, N$, over $\hat{\Omega}$ (see Figure 3) defined as

$$\xi_i = -\cos(i\pi/N) \qquad \eta_j = -\cos(j\pi/N) \tag{13}$$

The discrete solution of the 2-D problem is sought in the form of tensor product of one-dimensional expansions as follows

$$\begin{Bmatrix} \hat{u}^N \\ \hat{v}^N \end{Bmatrix} = \sum_{m=0}^{N}\sum_{n=0}^{N} \begin{Bmatrix} \hat{u}_{mn} \\ \hat{v}_{mn} \end{Bmatrix} \psi_m(\xi)\psi_n(\eta) \tag{14}$$

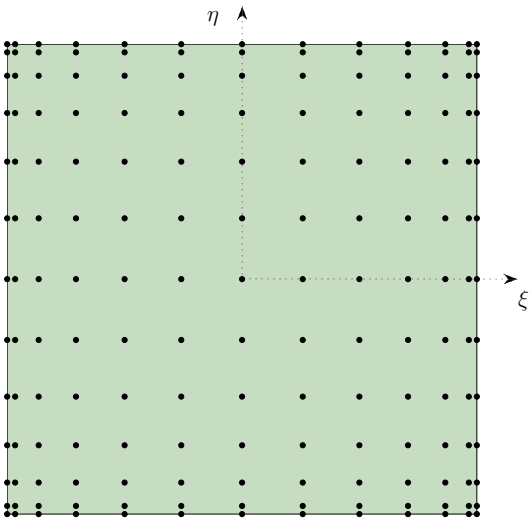

Figure 3: Two dimensional grid of Chebyshev-Gauss-Lobatto points on the computational domain (example with $N = 12$).

where $\hat{u}_{mn}$ and $\hat{v}_{mn}$ are the unknown values at the grid points, i.e., $\hat{u}_{mn} = \hat{u}^N(\xi_m, \eta_n)$ and $\hat{v}_{mn} = \hat{v}^N(\xi_m, \eta_n)$, and ψ_l $(l = 0, \ldots, N)$ denotes the Lagrange interpolating polynomial relative to the given set of CGL nodes, so that $\psi_m(\xi_i) = \delta_{mi}$ and $\psi_n(\eta_j) = \delta_{nj}$ for $i, j = 0, \ldots, N$. The approximation $(\hat{u}^N, \hat{v}^N)$ is found by collocation; that is, $(\hat{u}^N, \hat{v}^N)$ is required to satisfy the differential problem Eq. (9) along with the boundary conditions Eq. (12) at the CGL nodes. The derivatives in the differential operators $\hat{\mathcal{L}}_{ij}$ and $\hat{\mathcal{B}}_{ij}$ are approximated through the interpolation derivatives, corresponding to the evaluation at the grid points of the first- and second-order derivatives of the interpolants in Eq. (14).

For the sake of convenience, the collocation equations are written in a matrix form. To this aim, the vectors $\mathbf{u}, \mathbf{v} \in \mathbb{R}^{(N+1)^2}$ of displacement values $\hat{u}_{mn}$ and $\hat{v}_{mn}$ at the CGL nodes are introduced, e.g. $\mathbf{u} = (\hat{u}_{00}, \hat{u}_{01}, \ldots, \hat{u}_{0N}, \ldots, \hat{u}_{NN})$ and $\mathbf{v} = (\hat{v}_{00}, \hat{v}_{01}, \ldots, \hat{v}_{0N}, \ldots, \hat{v}_{NN})$. They are sorted so that increasing values of the coordinate ξ (η) starting from $\xi(\eta) = -1$ correspond to increasing values of the index i (j). Thus, the four corners of the computational domain in Figure 3 are numbered as follows: $(.)_{00}$ (bottom left), $(.)_{N0}$ (bottom right), $(.)_{0N}$ (top left), and $(.)_{NN}$ (top right). Similarly, the values of the derivatives at the CGL points are collected into vectors which are denoted by a subscript indicating the variable with respect of which the partial derivative is taken, i.e., $()_\xi = \partial/\partial\xi$. They can be expressed through the Kronecker

product $\otimes$ as follows

$$\begin{aligned}
\mathbf{u}_{\xi} &= \left(\mathbf{D}^{(1)} \otimes \mathbf{I}\right) \mathbf{u} & \mathbf{u}_{\eta\eta} &= \left(\mathbf{I} \otimes \mathbf{D}^{(2)}\right) \mathbf{u} \\
\mathbf{u}_{\eta} &= \left(\mathbf{I} \otimes \mathbf{D}^{(1)}\right) \mathbf{u} & \mathbf{v}_{\xi\xi} &= \left(\mathbf{D}^{(2)} \otimes \mathbf{I}\right) \mathbf{v} \\
\mathbf{v}_{\xi} &= \left(\mathbf{D}^{(1)} \otimes \mathbf{I}\right) \mathbf{v} & \mathbf{v}_{\eta\eta} &= \left(\mathbf{I} \otimes \mathbf{D}^{(2)}\right) \mathbf{v} \\
\mathbf{v}_{\eta} &= \left(\mathbf{I} \otimes \mathbf{D}^{(1)}\right) \mathbf{v} & \mathbf{u}_{\xi\eta} &= \left(\mathbf{D}^{(1)} \otimes \mathbf{D}^{(1)}\right) \mathbf{u} \\
\mathbf{u}_{\xi\xi} &= \left(\mathbf{D}^{(2)} \otimes \mathbf{I}\right) \mathbf{u} & \mathbf{v}_{\xi\eta} &= \left(\mathbf{D}^{(1)} \otimes \mathbf{D}^{(1)}\right) \mathbf{v}
\end{aligned}$$

where $\mathbf{I}$ is the identity matrix of size $(N+1)$, and $\mathbf{D}^{(1)}$ and $\mathbf{D}^{(2)}$ are the differentiation matrices containing, respectively, the first- and second-order derivatives of the interpolants evaluated at the CGL nodes. We have $\mathbf{D}^{(2)} = \left(\mathbf{D}^{(1)}\right)^2$ and the entries of $\mathbf{D}^{(1)}$ are reported for example in Refs. [27, 31].

By using the above notation, the discretized set of collocated equations of motions can be written as

$$\begin{bmatrix} \mathbf{L}_{11} & \mathbf{L}_{12} \\ \mathbf{L}_{21} & \mathbf{L}_{22} \end{bmatrix} \begin{Bmatrix} \mathbf{u} \\ \mathbf{v} \end{Bmatrix} = \lambda^2 \begin{Bmatrix} \mathbf{u} \\ \mathbf{v} \end{Bmatrix} \tag{15}$$

where

$$\begin{aligned}
\mathbf{L}_{11} &= -\frac{2+(1-\nu)\tan^2\alpha}{2}\left(\mathbf{D}^{(2)} \otimes \mathbf{I}\right) - \frac{1-\nu}{2}\frac{\phi^2}{\cos^2\alpha}\left(\mathbf{I} \otimes \mathbf{D}^{(2)}\right) \\
&\quad + (1-\nu)\phi\frac{\tan\alpha}{\cos\alpha}\left(\mathbf{D}^{(1)} \otimes \mathbf{D}^{(1)}\right) \\
\mathbf{L}_{12} &= -\frac{1+\nu}{2}\left[\phi\frac{1}{\cos\alpha}\left(\mathbf{D}^{(1)} \otimes \mathbf{D}^{(1)}\right) - \tan\alpha\left(\mathbf{D}^{(2)} \otimes \mathbf{I}\right)\right] \\
\mathbf{L}_{21} &= \mathbf{L}_{12} \\
\mathbf{L}_{22} &= -\frac{2\tan^2\alpha+1-\nu}{2}\left(\mathbf{D}^{(2)} \otimes \mathbf{I}\right) - \frac{\phi^2}{\cos^2\alpha}\left(\mathbf{I} \otimes \mathbf{D}^{(2)}\right) \\
&\quad + 2\phi\frac{\tan\alpha}{\cos\alpha}\left(\mathbf{D}^{(1)} \otimes \mathbf{D}^{(1)}\right)
\end{aligned} \tag{16}$$

The satisfaction of the equations of motion must be enforced at the interior CGL nodes only ($i, j = 1, \ldots, N-1$). Moreover, as it will be shown later, the boundary CGL points must be explicitly defined in order to connect the differential problem with the set of boundary conditions. To this aim, the following procedure is implemented. First, a matrix $\mathbf{Z}_I \in \mathbb{R}^{(N-1)^2 \times (N+1)^2}$ selecting the rows of the discrete operators

in Eq. (16) corresponding to interior points is introduced

$$\mathbf{Z}_I = \begin{bmatrix} \mathbf{e}^{\mathrm{T}}_{(N+1)+2} \\ \vdots \\ \mathbf{e}^{\mathrm{T}}_{2(N+1)-1} \\ \mathbf{e}^{\mathrm{T}}_{2(N+1)+2} \\ \vdots \\ \mathbf{e}^{\mathrm{T}}_{3(N+1)-1} \\ \vdots \end{bmatrix} \tag{17}$$

where $\mathbf{e}_i \in \mathbb{R}^{(N+1)^2 \times 1}$ is the ith unit vector, i.e., the vector which is zero in all entries except for the ith entry at which it is equal to 1. A similar selecting matrix $\mathbf{Z}_B \in \mathbb{R}^{4N \times (N+1)^2}$ corresponding to the boundary points is defined as

$$\mathbf{Z}_B = \begin{bmatrix} \mathbf{e}^{\mathrm{T}}_{1} \\ \vdots \\ \mathbf{e}^{\mathrm{T}}_{(N+1)} \\ \mathbf{e}^{\mathrm{T}}_{(N+1)+1} \\ \mathbf{e}^{\mathrm{T}}_{2(N+1)} \\ \vdots \\ \mathbf{e}^{\mathrm{T}}_{N(N+1)+1} \\ \vdots \\ \mathbf{e}^{\mathrm{T}}_{(N+1)(N+1)} \end{bmatrix} \tag{18}$$

Accordingly, Equations (15) are transformed into the following set

$$\mathbf{L}_B \mathbf{s}_B + \mathbf{L}_I \mathbf{s}_I = \lambda^2 \mathbf{s}_I \tag{19}$$

where

$$\mathbf{L}_B = \begin{bmatrix} \mathbf{Z}_I \mathbf{L}_{11} \mathbf{Z}_B^{\mathrm{T}} & \mathbf{Z}_I \mathbf{L}_{12} \mathbf{Z}_B^{\mathrm{T}} \\ \\ \mathbf{Z}_I \mathbf{L}_{21} \mathbf{Z}_B^{\mathrm{T}} & \mathbf{Z}_I \mathbf{L}_{22} \mathbf{Z}_B^{\mathrm{T}} \end{bmatrix} \tag{20}$$

$$\mathbf{L}_I = \begin{bmatrix} \mathbf{Z}_I \mathbf{L}_{11} \mathbf{Z}_I^{\mathrm{T}} & \mathbf{Z}_I \mathbf{L}_{12} \mathbf{Z}_I^{\mathrm{T}} \\ \\ \mathbf{Z}_I \mathbf{L}_{21} \mathbf{Z}_I^{\mathrm{T}} & \mathbf{Z}_I \mathbf{L}_{22} \mathbf{Z}_I^{\mathrm{T}} \end{bmatrix} \tag{21}$$

and

$$\mathbf{s}_I = \begin{Bmatrix} \mathbf{u}_I \\ \\ \mathbf{v}_I \end{Bmatrix} \qquad \mathbf{s}_B = \begin{Bmatrix} \mathbf{u}_B \\ \\ \mathbf{v}_B \end{Bmatrix}$$

are vectors containing displacement variables of interior and boundary points, respectively.

A similar procedure is employed for the discretization of the boundary conditions. Displacements and derivatives at the CGL boundary points along edge $\xi = -1$ are expressed as

$$\begin{aligned} \mathbf{u} &= \left(\mathbf{e}_1^{\mathrm{T}} \otimes \mathbf{I}\right) \mathbf{u} & \mathbf{v} &= \left(\mathbf{e}_1^{\mathrm{T}} \otimes \mathbf{I}\right) \mathbf{v} \\ \mathbf{u}_\xi &= \left(\mathbf{e}_1^{\mathrm{T}} \mathbf{D}^{(1)} \otimes \mathbf{I}\right) \mathbf{u} & \mathbf{v}_\xi &= \left(\mathbf{e}_1^{\mathrm{T}} \mathbf{D}^{(1)} \otimes \mathbf{I}\right) \mathbf{v} \\ \mathbf{u}_\eta &= \left(\mathbf{e}_1^{\mathrm{T}} \otimes \mathbf{D}^{(1)}\right) \mathbf{u} & \mathbf{v}_\eta &= \left(\mathbf{e}_1^{\mathrm{T}} \otimes \mathbf{D}^{(1)}\right) \mathbf{v} \end{aligned}$$

Similarly, for edge $\eta = -1$, we can write

$$\begin{aligned} \mathbf{u} &= \left(\mathbf{I} \otimes \mathbf{e}_1^{\mathrm{T}}\right) \mathbf{u} & \mathbf{v} &= \left(\mathbf{I} \otimes \mathbf{e}_1^{\mathrm{T}}\right) \mathbf{v} \\ \mathbf{u}_\xi &= \left(\mathbf{D}^{(1)} \otimes \mathbf{e}_1^{\mathrm{T}}\right) \mathbf{u} & \mathbf{v}_\xi &= \left(\mathbf{D}^{(1)} \otimes \mathbf{e}_1^{\mathrm{T}}\right) \mathbf{v} \\ \mathbf{u}_\eta &= \left(\mathbf{I} \otimes \mathbf{e}_1^{\mathrm{T}} \mathbf{D}^{(1)}\right) \mathbf{u} & \mathbf{v}_\eta &= \left(\mathbf{I} \otimes \mathbf{e}_1^{\mathrm{T}} \mathbf{D}^{(1)}\right) \mathbf{v} \end{aligned}$$

Related quantities referred to edges $\xi = 1$ and $\eta = 1$ are obtained from the previous expressions by substituting $\mathbf{e}_1$ with $\mathbf{e}_{N+1}$.

By using the above notation, the discretized set of boundary conditions for each of the four edges can be written as

$$\begin{bmatrix} \mathbf{B}_{11} & \mathbf{B}_{12} \\ \mathbf{B}_{21} & \mathbf{B}_{22} \end{bmatrix} \begin{Bmatrix} \mathbf{u} \\ \mathbf{v} \end{Bmatrix} = \begin{Bmatrix} \mathbf{0} \\ \mathbf{0} \end{Bmatrix} \qquad \text{(each edge)} \tag{22}$$

where the discrete operators $\mathbf{B}_{ij}$ are explicitly reported in Appendix C for the edge conditions considered in this work. The whole set of discretized boundary equations for all edges is then expressed in a more compact matrix form as follows

$$\begin{bmatrix} \mathbf{B}_\mathbf{u} & \mathbf{B}_\mathbf{v} \end{bmatrix} \begin{Bmatrix} \mathbf{u} \\ \mathbf{v} \end{Bmatrix} = \begin{Bmatrix} \mathbf{0} \\ \mathbf{0} \end{Bmatrix} \tag{23}$$

where $\mathbf{B}_\mathbf{u}$ collects the $\mathbf{B}_{11}$ and $\mathbf{B}_{21}$ matrices of the four edges related to the displacement vector $\mathbf{u}$ and $\mathbf{B}_\mathbf{v}$ groups together the $\mathbf{B}_{12}$ and $\mathbf{B}_{22}$ matrices of the four edges related to the displacement vector $\mathbf{v}$. Using vectors $\mathbf{s}_I$ and $\mathbf{s}_B$ of displacements at interior and boundary points, the boundary equations can be written as

$$\mathbf{B}_B \mathbf{s}_B + \mathbf{B}_I \mathbf{s}_I = \mathbf{0} \tag{24}$$

where

$$\mathbf{B}_B = \begin{bmatrix} \mathbf{B}_\mathbf{u} \mathbf{Z}_B^{\mathrm{T}} & \mathbf{B}_\mathbf{v} \mathbf{Z}_B^{\mathrm{T}} \end{bmatrix} \qquad \mathbf{B}_I = \begin{bmatrix} \mathbf{B}_\mathbf{u} \mathbf{Z}_I^{\mathrm{T}} & \mathbf{B}_\mathbf{v} \mathbf{Z}_I^{\mathrm{T}} \end{bmatrix} \tag{25}$$

2.4. Solution

The discretized problem is governed by Eqs. (19) and (24). From the second, we get

$$\mathbf{s}_B = -\mathbf{B}_B^{-1} \mathbf{B}_I \mathbf{s}_I \tag{26}$$

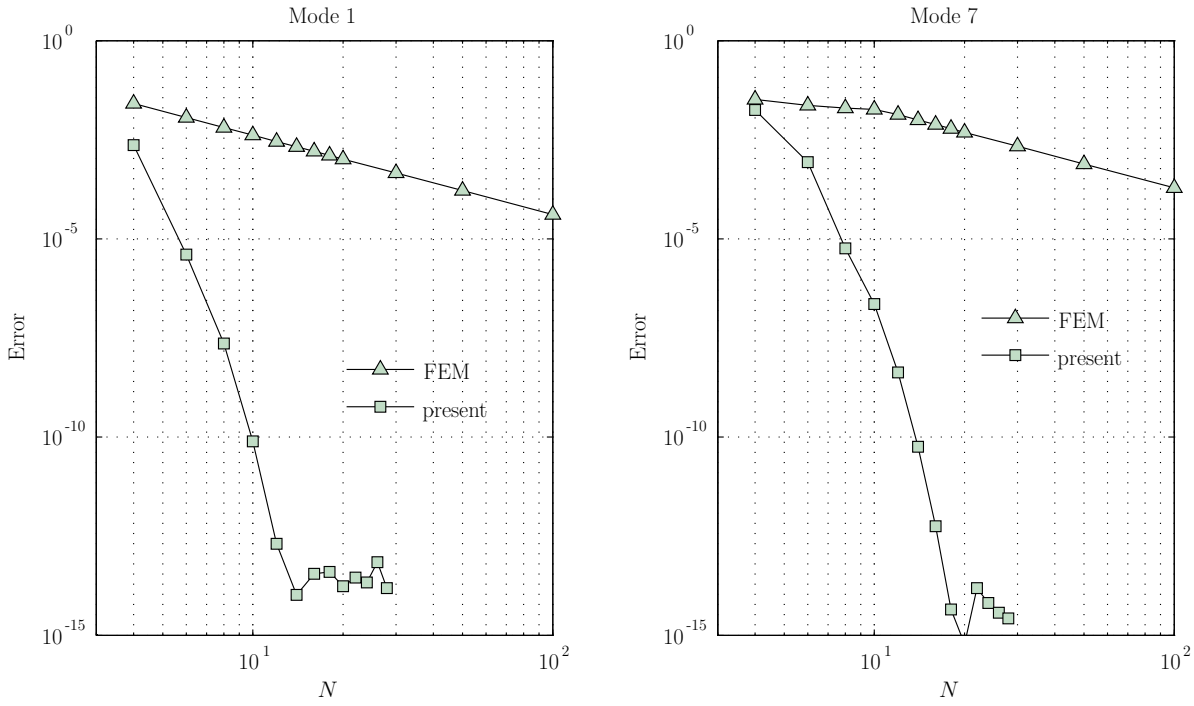

Figure 4: Convergence study for SS1-SS1-SS1-SS1 rectangular plate.

Substituting Eq. (26) into Eq. (19) yields the following standard eigenvalue problem

$$\left(\mathbf{L}_{\mathrm{I}} - \mathbf{L}_{\mathrm{B}}\mathbf{B}_{B}^{-1}\mathbf{B}_{I}\right)\mathbf{s}_{I} = \lambda^{2}\mathbf{s}_{I} \tag{27}$$

3. Numerical analysis

In this section, some illustrative numerical examples are presented to show the convergence rate and accuracy of the spectral collocation solution. In the following, the combination of edge conditions of the skew plate is represented by a compact four-letter symbolic notation for describing clamped (C), free (F), simply-supported of type 1 (SS1) and type 2 (SS2) boundary conditions, numbered in a counterclockwise direction beginning from edge DA (see Figure 2).

3.1. Convergence study

First, a rectangular plate ($\alpha = 0^{o}$) with $\phi = 0.833$ and two different sets of boundary conditions, SS1-SS1-SS1-SS1 and SS1-C-SS1-F, is considered. The present solution for increasing number N of CGL points is compared with the solution obtained using a classical FEM in Figures 4 and 5 for the fundamental mode and an arbitrarily selected higher-order mode (mode 7 for the fully simply-supported plate and mode 8 for the SS1-C-SS1-F plate). The error $|\omega - \omega_e|/\omega_e$ is shown, where ω_e is the reference exact value of the in-plane natural frequency as reported in Ref. [16]. We see, as expected, exponential convergence for the

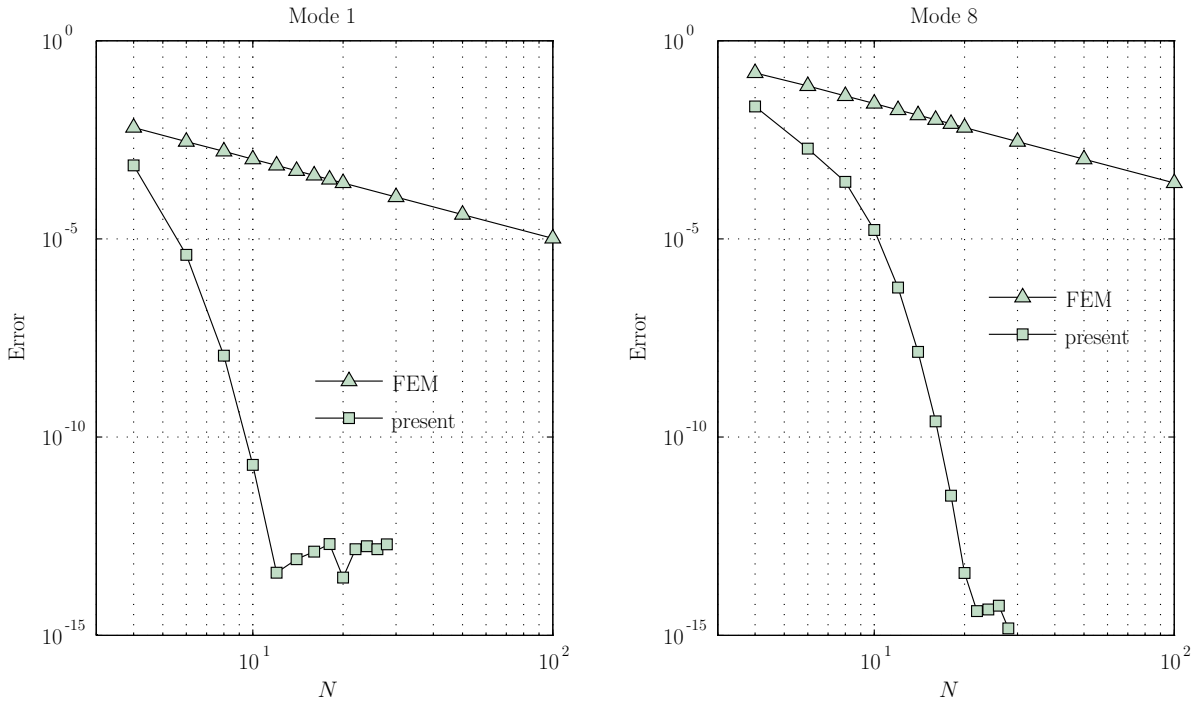

Figure 5: Convergence study for SS1-C-SS1-F rectangular plate.

spectral solutions, whereas the FE solutions are limited to algebraic convergence. Note that the deviations from the exact values are so small for $N \geq 20$ that they are swamped by the round-off error of the present computations. Furthermore, it is apparent that the convergence is not affected by the edge conditions of the rectangular plate.

The convergence rate of the method is then evaluated by varying the skew angle of the plate considered before, now having SS2-SS2-SS2-SS2 boundary conditions. The skew angle α is assumed to be equal to $0^o, 15^o, 30^o, 45^o$ and 75^o, ranging from a rectangular to a highly skewed plate. Figure 6 shows the value of $\Delta = |\omega^{N_{k+1}} - \omega^{N_k}|$ for two modes (mode 3 and mode 7) as function of increasing values of N. It is observed that the skewness of the plate largely affects the convergence of the spectral solution. Increasing angles slow down the rate of convergence since the solution is non-smooth due to the corner singularities.

Another case corresponding to a cantilever F-C-F-F plate with $\phi = 1.0$ is presented in Figure 7. It is noted that the convergence rate is negatively affected by the presence of free corners when the plate is rectangular ($\alpha = 0^o$). It is also observed that, even though the plate has free corners, a behaviour similar to the previous case (see Fig. 6) is obtained for nonzero skew angles. Due to the strong effect of the skewness of the plate with free corners on the rate of convergence of the spectral solution, one may question whether the present results obtained with a selected value N of collocation points are accurate. To answer this question, Table 1 shows the first six in-plane frequency parameters $\lambda = \omega a\sqrt{\rho/E}$ of a rhombic F-C-F-F plate with $\alpha = 75^o$ as a function of N. The eigenvalues are compared with those obtained from a finite

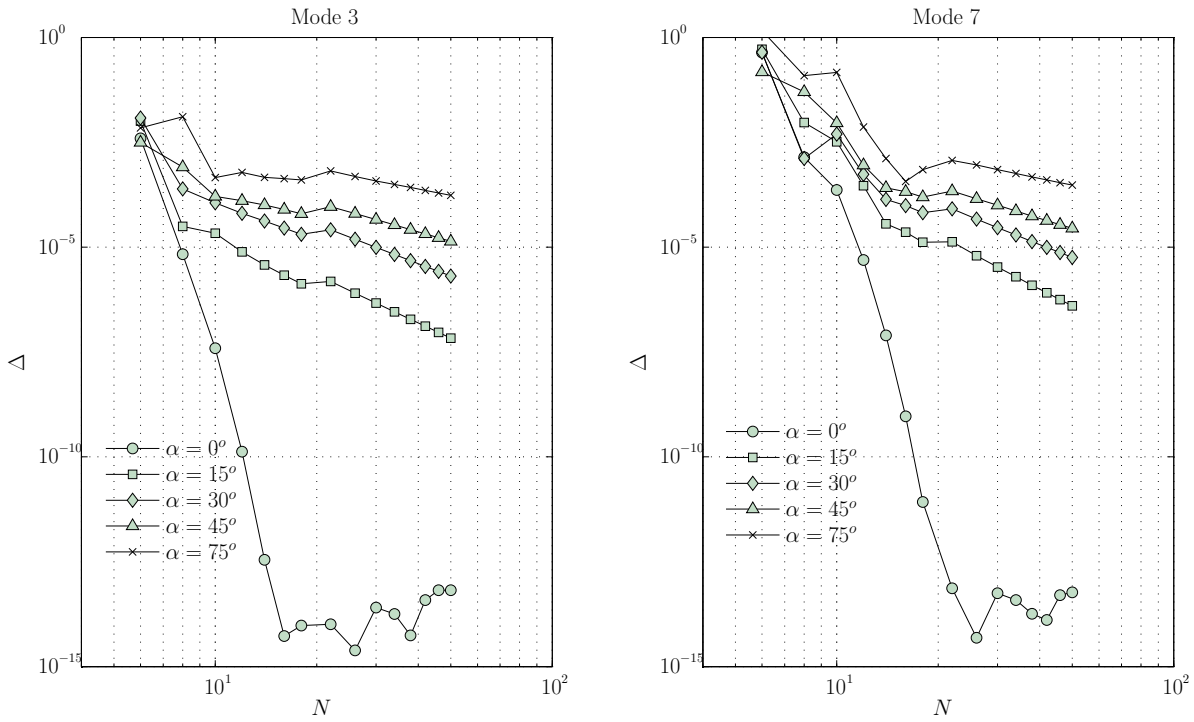

Figure 6: Convergence study for skew SS2-SS2-SS2-SS2 plates with $\phi = 1/1.2$.

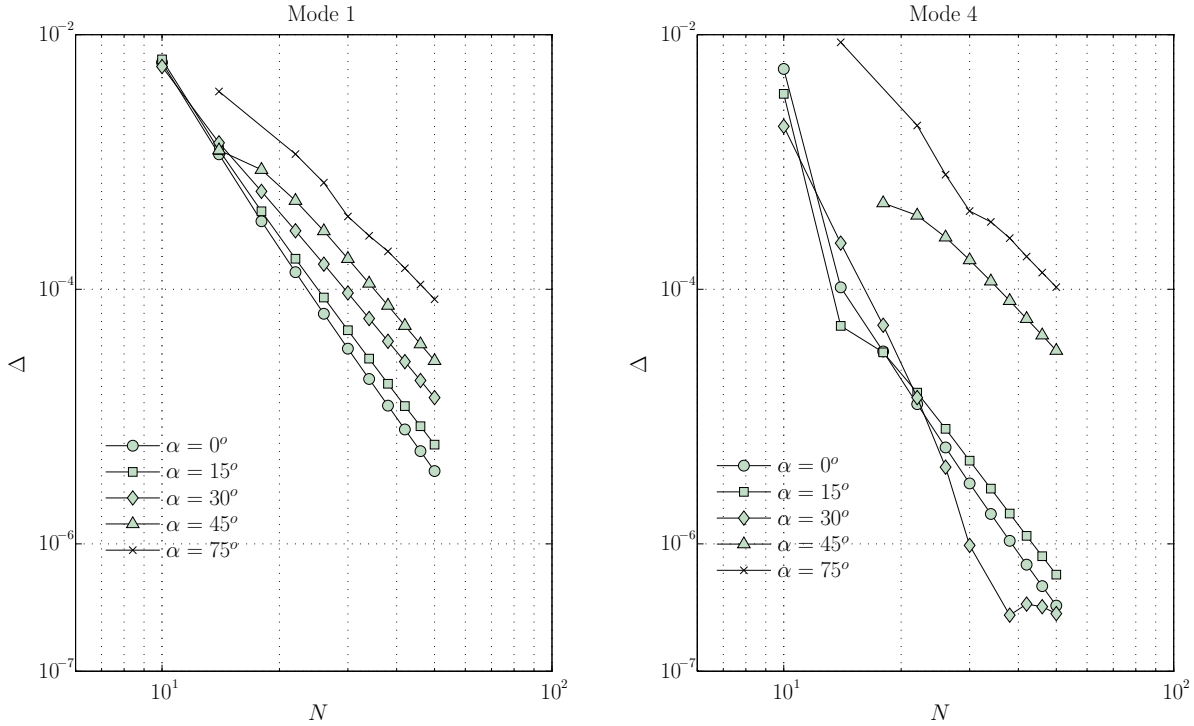

Figure 7: Convergence study for skew F-C-F-F plates with $\phi = 1.0$.

Table 1: First six in-plane frequency parameters $\lambda = \omega a\sqrt{\rho/E}$ of a rhombic F-C-F-F plate.

	Mode					
N	1	2	3	4	5	6
22	0.3502	0.9545	1.7113	2.0608	2.8895	3.9583
26	0.3495	0.9544	1.7080	2.0600	2.8885	3.9520
30	0.3491	0.9537	1.7058	2.0596	2.8866	3.9477
34	0.3489	0.9532	1.7043	2.0593	2.8851	3.9449
38	0.3487	0.9528	1.7032	2.0590	2.8840	3.9429
42	0.3485	0.9525	1.7025	2.0588	2.8831	3.9413
46	0.3484	0.9523	1.7018	2.0587	2.8824	3.9402
50	0.3483	0.9521	1.7014	2.0586	2.8818	3.9393
FEM	0.3484	0.9524	1.7003	2.0613	2.8952	3.9576
$err(\%)$	0.03	0.03	0.06	0.13	0.46	0.46

element model in ABAQUS with a refined mesh of 300×300 elements. The percentage error of the spectral solution computed with $N = 50$ with respect to the FE solution is also shown in the last row of the table. It is observed that the present converged values obtained using 50 collocation points in each plate direction are very close to the reference FE results. Rather accurate eigenfrequencies are also found when a relatively small number of collocation points are adopted.

The rate of convergence is also affected by the boundary conditions of the skew plate. This is shown in Figure 8 for a plate with $\phi = 0.833$ and $\alpha = 30^o$ having six different combinations of edge conditions.

The adversing effect of increasing skewness of the plate on the rate of convergence was also observed in previous studies dealing with transverse vibrations and buckling [32, 33] and it is still considered to be a challenge for numerical methods. From the previous analysis, it is noted that, although the exponential convergence of the spectral collocation solution is lost when skew plates are considered, well converged results to four significant digits are obtained in all cases when $N = 50$. Therefore, the frequency values shown in the following are considered to be highly accurate.

3.2. Comparison study

The accuracy of the present spectral solution is now explicitly evaluated and discussed by comparison with some exact and reference values available in the literature. As done previously, rectangular plates are considered first. Table 2 lists the first ten in-plane non dimensional frequency parameters $\lambda = \omega a/\pi c$ ($c = \sqrt{G/\rho}$ is the shear wave velocity and G is the shear modulus) of plates with aspect ratio $\phi = 0.833$ and various boundary conditions. Present results are computed with $N = 20$ CGL collocation points. Values in round brackets, when available, are taken from exact analysis presented in Ref. [16]. It can be noticed the excellent agreement of this solution and the exact eigenfrequencies, even when a relatively small number of collocation points is adopted.

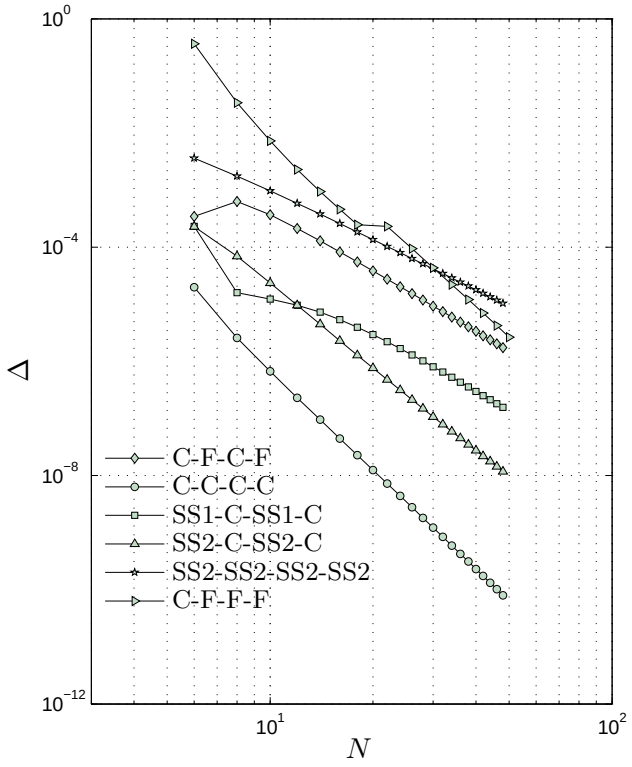

Figure 8: Convergence study for plates with $\phi = 1/1.2$, $\alpha = 30^o$ and various boundary conditions. Fundamental in-plane mode.

Table 2: First ten in-plane frequency parameters $\lambda = \omega a/\pi c$ of rectangular plates with $\phi = 0.8333$ and various boundary conditions. Comparison with exact solutions reported in Ref. [16].

	Mode									
Boundary conditions	1	2	3	4	5	6	7	8	9	10
SS1-SS1-SS1-SS1	0.8333	1.0000	1.3017	1.6667	1.9437	2.0000	2.1667	2.2003	2.5000	2.6034
	(0.8333)	(1.0000)	(1.3017)	(1.6667)	(1.9437)	(2.0000)	(2.1667)	(2.2003)	(2.5000)	(2.6034)
SS2-SS2-SS2-SS2	1.3017	1.4086	1.6903	1.9437	2.1667	2.2003	2.6034	2.6926	2.8172	3.1136
	(1.3017)	(1.4086)	(1.6903)	(1.9437)	(2.1667)	(2.2003)	(2.6034)	(2.6926)	(2.8172)	(3.1136)
SS1-C-SS1-C	0.8333	1.5406	1.6667	1.7846	2.2493	2.3915	2.5000	2.5735	2.7774	3.1512
	(0.8333)	(1.5406)	(1.6667)	(1.7846)	(2.2493)	(2.3915)	(2.5000)	(2.5735)	(2.7774)	(–)
SS2-C-SS2-C	1.4086	1.5406	1.7846	2.2493	2.3915	2.5735	2.7774	2.8172	3.1512	3.3292
	(1.4086)	(1.5406)	(1.7846)	(2.2493)	(2.3915)	(2.5735)	(2.7774)	(–)	(–)	(–)
SS1-C-SS1-F	0.4167	0.9970	1.2500	1.5900	1.8388	2.0492	2.0783	2.0833	2.3976	2.7491
	(0.4167)	(0.9970)	(1.2500)	(1.5900)	(1.8388)	(2.0492)	(2.0783)	(2.0833)	(–)	(–)
SS2-C-SS2-F	0.7043	0.9970	1.5900	1.8388	2.0492	2.0783	2.1129	2.3976	2.7491	2.8321
	(0.7043)	(0.9970)	(1.5900)	(1.8388)	(2.0492)	(2.0783)	(2.1129)	(–)	(–)	(–)
SS1-C-SS2-F	0.7359	0.9029	1.3971	1.5252	1.9594	2.0398	2.2923	2.4121	2.5657	2.6312
	(0.7359)	(0.9029)	(1.3971)	(1.5252)	(1.9594)	(2.0398)	(2.2923)	(2.4121)	(2.5657)	(2.6312)

Table 3: First six in-plane frequency parameters $\lambda = \omega a\sqrt{\rho(1-\nu^2)/E}$ of fully clamped rectangular plates with various aspect ratios ϕ.

		Mode					
$\phi = a/b$	Source	1	2	3	4	5	6
1.0	Present	3.5552	3.5552	4.2350	5.1857	5.8586	5.8944
	Ref. [12]	3.554	3.554	4.236	5.185	5.859	5.896
	Ref. [3]	3.555	3.555	4.235	5.186	5.859	5.895
	Ref. [6]	3.5552	3.5552	4.2350	5.1859	5.8587	5.8946
1.5	Present	4.1127	4.9252	5.4024	6.5644	6.6024	6.6164
	Ref. [12]	4.112	4.923	5.402	6.564	6.602	6.617
2.0	Present	4.7890	6.3786	6.7121	7.0488	7.6083	8.1402
	Ref. [12]	4.788	6.374	6.710	7.048	7.608	8.140
	Ref. [3]	4.789	6.379	6.712	7.049	7.608	8.140
2.5	Present	5.5398	7.5911	7.8744	8.1011	8.7759	9.5653
	Ref. [12]	5.538	7.590	7.868	8.097	8.773	9.568
3.0	Present	6.3385	8.1970	9.3950	9.5398	10.056	10.543
	Ref. [12]	6.336	8.195	9.385	9.532	10.05	10.54

Another case is considered in Table 3, where the first six in-plane nondimensional frequency parameters $\lambda = \omega a\sqrt{\rho(1-\nu^2)/E}$ of fully clamped rectangular plates with various aspect ratios ϕ are tabulated. As before, the present solutions are computed with $N = 20$. Comparison with other approximate solutions obtained using analytical-type methods is reported. Again, the spectral collocation method is capable of providing highly accurate eigenvalues in the overall frequency range of interest.

Finally, the present numerical approach is compared with the energy method proposed by Singh *et al.* [7] to compute the in-plane natural frequencies corresponding to the first six modes of rhombic ($\phi = 1.0$) skew plates having three different combinations of clamped and free edge conditions. Nondimensional frequency parameters $\lambda = \omega a\sqrt{\rho/E}$ are reported in Table 4 for skew angle $\alpha = 0^o, 15^o, 30^o, 45^o$ and 60^o. As suggested by the convergence analysis discussed above, accurate converged eigenvalues of plates with increasing skew angle require the use of an increasing number of collocation points. For this reason, the present solutions are computed with $N = 50$. We see from Table 4 a good agreement between the two methods for small skew angles. When $\alpha > 30^o$, a slightly increasing discrepancy is observed. This is probably due to the limited number of degrees of freedom of the discretized model developed in Ref. [7]. Indeed, no convergence study is reported in the work of Singh *et al.* to evaluate the degree of accuracy of the adopted truncated model. Since their approach can be classified as an energy method based on a Ritz approximation, the frequency values computed in Ref. [7] are upper-bound solutions of the in-plane free vibration problem. Therefore, it is believed that the present solutions have an higher degree of accuracy with respect to the comparison results.

Table 4: First six in-plane frequency parameters $\lambda = \omega a\sqrt{\rho/E}$ of rhombic skew plates with various boundary conditions. Comparison with approximate solutions reported in Ref. [7].

		Skew angle α				
Boundary conditions	Mode	0^o	15^o	30^o	45^o	60^o
C-C-C-C	1	3.7269	3.6814	3.8498	4.3406	5.5368
		(3.7270)	(3.6814)	(3.8498)	(4.3407)	(5.5372)
	2	3.7269	3.9741	4.4856	5.4574	7.5134
		(3.7270)	(3.9743)	(4.4861)	(5.4588)	(7.5428)
	3	4.4395	4.5708	5.0125	5.9590	7.5420
		(4.4395)	(4.5708)	(5.0125)	(5.9608)	(7.5231)
	4	5.4361	5.4860	5.6950	6.2328	8.0486
		(5.4363)	(5.4862)	(5.6953)	(6.2334)	(8.0737)
	5	6.1415	6.1668	6.5249	7.4379	9.3357
		(6.1601)	(6.1674)	(6.5262)	(7.4494)	(9.3394)
	6	6.1790	6.2888	6.7838	7.8431	9.5452
		(6.1741)	(6.2888)	(6.7847)	(7.9611)	(9.7038)
C-C-C-F	1	2.3794	2.4376	2.6321	3.0435	3.9231
		(2.3801)	(2.4390)	(2.6360)	(3.0521)	(3.9428)
	2	3.3156	3.3850	3.6138	4.0918	5.1234
		(3.3165)	(3.3865)	(3.6174)	(4.1027)	(5.1716)
	3	3.5735	3.6659	3.9724	4.5979	5.8302
		(3.5742)	(3.6678)	(3.9792)	(4.6204)	(5.9077)
	4	4.5137	4.5560	4.7437	5.2288	6.4238
		(4.5148)	(4.5572)	(4.7449)	(5.2293)	(6.4405)
	5	4.9459	5.0885	5.4610	6.1020	7.4825
		(4.9459)	(5.0827)	(5.1358)	(6.1184)	(7.6716)
	6	5.1969	5.2630	5.6160	6.4744	7.8463
		(5.1970)	(5.2633)	(5.6158)	(6.4821)	(7.9042)
C-F-C-F	1	1.7747	1.8258	1.9965	2.3576	3.1361
		(1.7758)	(1.8283)	(2.0040)	(2.3776)	(3.1955)
	2	3.1635	3.2315	3.4586	3.9373	4.9110
		(3.1653)	(3.2360)	(3.4737)	(3.7975)	(4.9137)
	3	3.2711	3.3225	3.5191	3.9727	4.9654
		(3.2713)	(3.3225)	(3.5010)	(3.9587)	(5.0550)
	4	3.5125	3.6054	3.8485	4.2483	5.1440
		(3.5130)	(3.6059)	(3.8486)	(4.2501)	(5.1719)
	5	3.9238	4.0045	4.3170	4.8266	5.9043
		(3.9266)	(4.0097)	(4.3282)	(4.8358)	(5.9619)
	6	4.0908	4.1488	4.3553	5.0415	6.4774
		(4.0912)	(4.1498)	(4.3569)	(5.0693)	(6.5640)

Table 5: Fundamental in-plane frequency parameter $\lambda = \omega a/\pi c$ of SS1-C-SS1-C plates with various aspect ratios $\phi = a/b$ and skew angles α.

	Skew angle α				
Aspect ratio ϕ	0^o	15^o	30^o	45^o	60^o
1.0	1.0000	1.0370	1.1602	1.4199	1.9820
1.5	1.5000	1.5567	1.7460	2.1474	3.0245
2.0	2.0000	2.0745	2.3238	2.8543	4.0230
2.5	2.5000	2.5922	2.9010	3.5607	5.0222
3.0	3.0000	3.1098	3.4782	4.2674	6.0217

Table 6: Fundamental in-plane frequency parameter $\lambda = \omega a/\pi c$ of SS2-C-SS2-C plates with various aspect ratios $\phi = a/b$ and skew angles α.

	Skew angle α				
Aspect ratio ϕ	0^o	15^o	30^o	45^o	60^o
1.0	1.6903	1.6624	1.6637	1.7618	2.0709
1.5	2.1976	2.1940	2.2495	2.4653	3.0608
2.0	2.5676	2.6072	2.7595	3.1376	4.0586
2.5	2.9746	3.0404	3.2731	3.8089	5.0567
3.0	3.4060	3.4940	3.7991	4.4849	6.0548

3.3. Parametric study

The last numerical analysis presented in this work refers to some new frequency values corresponding to the in-plane fundamental mode of plates with different skew angles, aspect ratios, and boundary conditions, with the aim of covering a reasonably complete set of application cases. The skew angle is varied from 0^o to 60^o with a step of 15^o. The analysis includes plates with aspect ratio $\phi = 1.0, 1.5, 2.0, 2.5$ and 3.0. Five combinations of boundary conditions are considered in Tables 5 to 9 comprising SS1-C-SS1-C, SS2-C-SS2-C, C-C-C-C, C-C-C-F, and C-F-C-F plates. The non dimensional in-plane natural frequency $\lambda = \omega a/\pi c$ is shown in all cases as a result of computations performed with 50 collocation points. The following

Table 7: Fundamental in-plane frequency parameter $\lambda = \omega a/\pi c$ of C-C-C-C plates with various aspect ratios $\phi = a/b$ and skew angles α.

	Skew angle α				
Aspect ratio ϕ	0^o	15^o	30^o	45^o	60^o
1.0	1.9128	1.8895	1.9759	2.2279	2.8418
1.5	2.2128	2.2548	2.4060	2.7561	3.5796
2.0	2.5767	2.6376	2.8479	3.3191	4.4170
2.5	2.9807	3.0594	3.3296	3.9299	5.3211
3.0	3.4104	3.5072	3.8383	4.5706	6.2599

Table 8: Fundamental in-plane frequency parameter $\lambda = \omega a/\pi c$ of C-C-C-F plates with various aspect ratios $\phi = a/b$ and skew angles α.

	Skew angle α				
Aspect ratio ϕ	0^o	15^o	30^o	45^o	60^o
1.0	1.2213	1.2511	1.3510	1.5621	2.0136
1.5	1.5015	1.5373	1.6558	1.8989	2.3887
2.0	1.8374	1.8687	1.9750	2.2054	2.7263
2.5	2.0465	2.0751	2.1862	2.4514	3.0876
3.0	2.2072	2.2468	2.3874	2.7117	3.4883

Table 9: Fundamental in-plane frequency parameter $\lambda = \omega a/\pi c$ of C-F-C-F plates with various aspect ratios $\phi = a/b$ and skew angles α.

	Skew angle α				
Aspect ratio ϕ	0^o	15^o	30^o	45^o	60^o
1.0	0.9109	0.9372	1.0248	1.2101	1.6096
1.5	0.8637	0.8827	0.9437	1.0607	1.2604
2.0	0.8128	0.8252	0.8631	0.9250	0.9919
2.5	0.7606	0.7678	0.7879	0.8117	0.8046
3.0	0.7095	0.7127	0.7195	0.7173	0.6698

observations can be made from tabulated values:

1. the fundamental in-plane frequency of SS1-C-SS1-C plates increases significantly as the skew angle and aspect ratio increase;
2. the same behavior as above occurs for SS2-C-SS2-C plates, but the increment of the fundamental eigenvalue is less marked;
3. fully clamped plates exhibit frequency values close to those of SS2-C-SS2-C plates at high aspect ratios;
4. the first in-plane frequency of C-F-C-F plates decreases with increasing aspect ratio; it is also noted in this case that, for aspect ratios up to 2, the frequency monotonically increases as the skew angle increases; instead, for higher values of the aspect ratio, there is first an increasing and then a decreasing behavior.

The above informations can be useful in the design process and the accurate results reported in the Tables can be also used as benchmark values for validating other numerical techniques aimed at solving the in-plane free vibration problem of skew plates.

4. Conclusions

The paper has presented the solution of the free in-plane vibration problem for isotropic skew plates with arbitrary combination of classical boundary conditions using the spectral collocation method. Rectangular plates are also included in the analysis as a particular case when the skew angle is set to zero. Results for different skew angles and aspect ratios are reported and discussed. It is shown that the spectral collocation method exhibits a good rate of convergence as the number of collocation points increases and provides frequency values with a high degree of accuracy. Some design guidelines are also provided by studying the effect of the plate geometry on the variation of the fundamental eigenvalue. A rather comprehensive set of new accurate results is presented, which can be used as a reference for future numerical studies. It is believed that the present work contributes in extending the available studies on the in-plane vibration of plates with non-rectangular shape.

References

[1] R.H. Lyon, In-plane contribution to structural noise transmission, *Noise Control Engineering*, 26 (1986), 22-27.

[2] R.S. Langley, A.N. Bercin, Wave intensity analysis of high frequency vibrations, *Philosophical Transactions of the Royal Society A*, 1994, 489-499.

[3] N.S. Bardell, R.S. Langley, J.M. Dunsdon, On the free in-plane vibration of isotropic rectangular plates, *Journal of Sound and Vibration*, 191 (1996), 459-467.

[4] R.L. Woodcock, R.B. Bhat, I.G. Stiharu, Effect of ply orientation on the in-plane vibration of single-layer composite plates, *Journal of Sound and Vibration*, 312 (2008), 94-108.

[5] L. Dozio, In-plane free vibrations of single-layer and symmetrically laminated rectangular composite plates, *Composite Structures*, 93 (2011), 1787-1800.

[6] L. Dozio, Free in-plane vibration analysis of rectangular plates with arbitrary elastic boundaries, *Mechanics Research Communications*, 37 (2010), 627-635.

[7] A.V. Singh, T. Muhammad, Free in-plane vibration of isotropic non-rectangular plates, *Journal of Sound and Vibration*, 273 (2004), 219-231.

[8] D.J. Gorman, Free in-plane vibration analysis of rectangular plates by the method of superposition, *Journal of Sound and Vibration*, 272 (2004), 831-851.

[9] D.J. Gorman, Accurate analytical-type solutions for the free in-plane vibration of clamped and simply supported rectangular plates, *Journal of Sound and Vibration*, 276 (2004), 311-333.

[10] D.J. Gorman, Free in-plane vibration analysis of rectangular plates with elastic support normal to the boundaries, *Journal of Sound and Vibration*, 285 (2005), 941-966.

[11] G. Wang, N.M. Wereley, Free in-plane vibration of rectangular plates, *AIAA Journal*, 40 (2002), 953-959.

[12] J. Du, W.L. Li, G. Jin, T. Yang, Z. Liu, An analytical method for the in-plane vibration analysis of rectangular plates with elastically restrained edges, *Journal of Sound and Vibration*, 306 (2007), 908-927.

[13] Y. Zhang, J. Du, T. Yang, Z. Liu, A series solution for the in-plane vibration analysis of orthotropic rectangular plates with elastically restrained edges, *International Journal of Mechanical Sciences*, 79 (2014), 15-24.

[14] D. Shi, Q. Wang, X. Shi, F. Pang, A series solution for the in-plane vibration analysis of orthotropic rectangular plates with non-uniform elastic boundary constraints and internal line supports, *Archive of Applied Mechanics*, in press, 2014.

[15] D.J. Gorman, Exact solutions for the free in-plane vibration of rectangular plates with two opposite edges simply supported, *Journal of Sound and Vibration*, 294 (2006), 131-161.

[16] Y.F. Xing, B. Liu, Exact solutions for the free in-plane vibrations of rectangular plates, *International Journal of Mechanical Sciences*, 51 (2009), 246-255.

[17] B. Liu, Y.F. Xing, Comprehensive exact solutions for free in-plane vibrations of orthotropic rectangular plates, *European Journal of Mechanics - A/Solids*, 30 (2011), 383-395.

[18] L. Zhou, W.X. Zheng, Vibration of skew plates by the MLS-Ritz method, *International Journal of Mechanical Sciences*, 50 (2008), 1133-1141.

[19] X. Wang, Y. Wang, Z. Yuan, Accurate vibration analysis of skew plates by the new version of the differential quadrature method, *Applied Mathematical Modelling*, 38 (2014), 926-937.

[20] C. Canuto, M.Y. Hussaini, A. Quarteroni, T.A. Zang, *Spectral Methods - Fundamentals in Single Domains*, Springer, Berlin, 2006.

[21] B. Fornberg, *A Practical Guide to Pseudospectral Methods*, Cambridge University Press, 1996.

[22] C. Lin, M. Jen, Analysis of a laminated anisotropic plate by Chebyshev collocation method, *Composites Part B*, 36 (2005), 155-169.

[23] J. Lee, W.W. Schultz, Eigenvalue analysis of Timoshenko beams and axisymmetric Mindlin plates by the pseudospectral method, *Journal of Sound and Vibration*, 269 (2004), 609-621.

[24] M. S. Sari, E. A. Butcher, Effects of damaged boundaries on the free vibration of Kirchhoff plates: comparison of perturbation and spectral collocation solutions, *Journal of Computational and Nonlinear Dynamics*, 7 (2012), 011011.

[25] M. S. Sari, E. A. Butcher, Free vibration analysis of rectangular and annular Mindlin plates with undamaged and damaged boundaries by the spectral collocation method, *Journal of Vibration and Control*, 18 (2011), 1722-1736.

[26] M. S. Sari, E. A. Butcher, Three Dimensional Vibration Analysis of Rectangular Plates with Undamaged and Damaged Boundaries by the Spectral Collocation Method, *International Journal of Acoustics and Vibration*, 19 (2014), 3-9.

[27] C. Shu, *Differential Quadrature and Its Application in Engineering*, Springer, London, 2000.

[28] C.W. Bert, M. Malik, Differential quadrature method in computational mechanics: a review, *Applied Mechanics Review*, 49 (1996), 1-28.

[29] M. Malik, C.W. Bert, Implementing multiple boundary conditions in the DQ solution of higher-order PDEs: application to free vibration of plates, *International Journal for Numerical Methods in Engineering*, 39 (1996), 1237-1258.

[30] G. Karami, P. Malekzadeh, Application of a new differential quadrature methodology for free vibration analysis of plates, *International Journal for Numerical Methods in Engineering*, 56 (2003), 847-868.

[31] J.A.C. Weideman, S.C. Reddy, A MATLAB differentiation matrix suite, *ACM Transactions on Mathematical Software*, 26 (2000), 465-519.

[32] O.G. McGee, A.W. Leissa, C.S. Huang, Vibrations of cantilevered skewed trapezoidal and triangular plates with corner stress singularities, *International Journal of Mechanical Sciences*, 34 (1992), 63-84.

[33] W.X. Wu, C. Shu, C.M. Wang, Y.Xiang, Free vibration and buckling analysis of highly skewed plates by least-squares based finite difference method, *International Journal of Structural Stability and Dynamics*, 10 (2010), 225-252.

Appendix A

The boundary operators in Eq. (6) are defined below for each in-plane classical boundary condition considered in this work:

- clamped ($u_n = 0$, $u_s = 0$):

$$\begin{aligned}
\mathcal{B}_{11} &= n_x \\
\mathcal{B}_{12} &= n_y \\
\mathcal{B}_{21} &= n_y \\
\mathcal{B}_{22} &= -n_x
\end{aligned} \tag{28}$$

- free ($N_{nn} = 0$, $N_{ns} = 0$):

$$\begin{aligned}
\mathcal{B}_{11} &= \left(A_{11}n_x^2 + A_{12}n_y^2\right)\frac{\partial}{\partial x} + 2A_{66}n_x n_y\frac{\partial}{\partial y} \\
\mathcal{B}_{12} &= \left(A_{12}n_x^2 + A_{22}n_y^2\right)\frac{\partial}{\partial y} + 2A_{66}n_x n_y\frac{\partial}{\partial x} \\
\mathcal{B}_{21} &= \left(A_{12} - A_{11}\right)n_x n_y\frac{\partial}{\partial x} + A_{66}\left(n_x^2 - n_y^2\right)\frac{\partial}{\partial y} \\
\mathcal{B}_{22} &= \left(A_{22} - A_{12}\right)n_x n_y\frac{\partial}{\partial y} + A_{66}\left(n_x^2 - n_y^2\right)\frac{\partial}{\partial x}
\end{aligned} \tag{29}$$

- simply supported - type 1 ($u_s = 0$, $N_{nn} = 0$):

$$\begin{aligned}
\mathcal{B}_{11} &= n_y \\
\mathcal{B}_{12} &= -n_x \\
\mathcal{B}_{21} &= \left(A_{11}n_x^2 + A_{12}n_y^2\right)\frac{\partial}{\partial x} + 2A_{66}n_x n_y\frac{\partial}{\partial y} \\
\mathcal{B}_{22} &= \left(A_{12}n_x^2 + A_{22}n_y^2\right)\frac{\partial}{\partial y} + 2A_{66}n_x n_y\frac{\partial}{\partial x}
\end{aligned} \tag{30}$$

- simply supported - type 2 ($u_n = 0$, $N_{ns} = 0$):

$$\begin{aligned}
\mathcal{B}_{11} &= n_x \\
\mathcal{B}_{12} &= n_y \\
\mathcal{B}_{21} &= \left(A_{12} - A_{11}\right)n_x n_y\frac{\partial}{\partial x} + A_{66}\left(n_x^2 - n_y^2\right)\frac{\partial}{\partial y} \\
\mathcal{B}_{22} &= \left(A_{22} - A_{12}\right)n_x n_y\frac{\partial}{\partial y} + A_{66}\left(n_x^2 - n_y^2\right)\frac{\partial}{\partial x}
\end{aligned} \tag{31}$$

Appendix B

The boundary operators in Eq. (12) are defined below according to the boundary conditions of each edge of the skew plate:

- clamped edge (C):

$$\begin{aligned}
\hat{\mathcal{B}}_{11} &= n_x \\
\hat{\mathcal{B}}_{12} &= n_y \\
\hat{\mathcal{B}}_{21} &= n_y \\
\hat{\mathcal{B}}_{22} &= -n_x
\end{aligned} \tag{32}$$

- free edge (F):

$$\begin{aligned}
\hat{\mathcal{B}}_{11} &= \left[\left(n_x^2 + \nu n_y^2\right) - (1-\nu)\tan\alpha\, n_x n_y\right]\frac{\partial}{\partial\xi} \\
&\quad + \frac{\phi}{\cos\alpha}(1-\nu)n_x n_y\frac{\partial}{\partial\eta} \\
\hat{\mathcal{B}}_{12} &= \left[-\tan\alpha\left(\nu n_x^2 + n_y^2\right) + (1-\nu)n_x n_y\right]\frac{\partial}{\partial\xi} \\
&\quad + \frac{\phi}{\cos\alpha}\left(\nu n_x^2 + n_y^2\right)\frac{\partial}{\partial\eta} \\
\hat{\mathcal{B}}_{21} &= \left[(\nu-1)n_x n_y - \tan\alpha\frac{1-\nu}{2}\left(n_x^2 - n_y^2\right)\right]\frac{\partial}{\partial\xi} \\
&\quad + \frac{\phi}{\cos\alpha}\frac{1-\nu}{2}\left(n_x^2 - n_y^2\right)\frac{\partial}{\partial\eta} \\
\hat{\mathcal{B}}_{22} &= \left[-\tan\alpha(1-\nu)n_x n_y + \frac{1-\nu}{2}\left(n_x^2 - n_y^2\right)\right]\frac{\partial}{\partial\xi} \\
&\quad + \frac{\phi}{\cos\alpha}(1-\nu)n_x n_y\frac{\partial}{\partial\eta}
\end{aligned} \tag{33}$$

- simply-supported type 1 edge (SS1):

$$\begin{aligned}
\hat{\mathcal{B}}_{11} &= n_y \\
\hat{\mathcal{B}}_{12} &= -n_x \\
\hat{\mathcal{B}}_{21} &= \left[\left(n_x^2 + \nu n_y^2\right) - (1-\nu)\tan\alpha\, n_x n_y\right]\frac{\partial}{\partial\xi} \\
&\quad + \frac{\phi}{\cos\alpha}(1-\nu)n_x n_y\frac{\partial}{\partial\eta} \\
\hat{\mathcal{B}}_{22} &= \left[-\tan\alpha\left(\nu n_x^2 + n_y^2\right) + (1-\nu)n_x n_y\right]\frac{\partial}{\partial\xi} \\
&\quad + \frac{\phi}{\cos\alpha}\left(\nu n_x^2 + n_y^2\right)\frac{\partial}{\partial\eta}
\end{aligned} \tag{34}$$

- simply-supported type 2 edge (SS2):

$$\begin{aligned}
\hat{\mathcal{B}}_{11} &= n_x \\
\hat{\mathcal{B}}_{12} &= n_y \\
\hat{\mathcal{B}}_{21} &= \left[(\nu-1)n_x n_y - \tan\alpha \frac{1-\nu}{2}\left(n_x^2 - n_y^2\right)\right]\frac{\partial}{\partial\xi} \\
&\quad + \frac{\phi}{\cos\alpha}\frac{1-\nu}{2}\left(n_x^2 - n_y^2\right)\frac{\partial}{\partial\eta} \\
\hat{\mathcal{B}}_{22} &= \left[-\tan\alpha(1-\nu)n_x n_y + \frac{1-\nu}{2}\left(n_x^2 - n_y^2\right)\right]\frac{\partial}{\partial\xi} \\
&\quad + \frac{\phi}{\cos\alpha}(1-\nu)n_x n_y \frac{\partial}{\partial\eta}
\end{aligned} \tag{35}$$

By referring to Figure 2, the components of the outward normal can be specified for the four edges as follows:

- edge DA: $n_x = \cos(\pi - \alpha) \qquad n_y = \sin(\pi - \alpha)$

- edge AB: $n_x = 0 \qquad n_y = -1$

- edge BC: $n_x = \cos(2\pi - \alpha) \qquad n_y = \sin(2\pi - \alpha)$

- edge CD: $n_x = 0 \qquad n_y = 1$

When $\alpha = 0$, the particular case of a rectangular plate is obtained.

Appendix C

The boundary operators in Eq. (22) are defined below according to the boundary conditions of each edge of the skew plate:

- edge DA, clamped

$$\begin{aligned}
\mathbf{B}_{11} &= n_x \left(\mathbf{e}_1^{\mathrm{T}} \otimes \mathbf{I}\right) \\
\mathbf{B}_{12} &= n_y \left(\mathbf{e}_1^{\mathrm{T}} \otimes \mathbf{I}\right) \\
\mathbf{B}_{21} &= n_y \left(\mathbf{e}_1^{\mathrm{T}} \otimes \mathbf{I}\right) \\
\mathbf{B}_{22} &= -n_x \left(\mathbf{e}_1^{\mathrm{T}} \otimes \mathbf{I}\right)
\end{aligned} \tag{36}$$

- edge DA, free

$$
\begin{aligned}
\mathbf{B}_{11} &= \left[\left(n_x^2+\nu n_y^2\right)-(1-\nu)\tan\alpha\, n_x n_y\right]\left(\mathbf{e}_1^{\mathrm{T}}\mathbf{D}^{(1)}\otimes\mathbf{I}\right)\\
&\quad+\frac{\phi}{\cos\alpha}(1-\nu)n_x n_y\left(\mathbf{e}_1^{\mathrm{T}}\otimes\mathbf{D}^{(1)}\right)\\
\mathbf{B}_{12} &= \left[-\tan\alpha\left(\nu n_x^2+n_y^2\right)+(1-\nu)n_x n_y\right]\left(\mathbf{e}_1^{\mathrm{T}}\mathbf{D}^{(1)}\otimes\mathbf{I}\right)\\
&\quad+\frac{\phi}{\cos\alpha}\left(\nu n_x^2+n_y^2\right)\left(\mathbf{e}_1^{\mathrm{T}}\otimes\mathbf{D}^{(1)}\right)\\
\mathbf{B}_{21} &= \left[(\nu-1)n_x n_y-\tan\alpha\frac{1-\nu}{2}\left(n_x^2-n_y^2\right)\right]\left(\mathbf{e}_1^{\mathrm{T}}\mathbf{D}^{(1)}\otimes\mathbf{I}\right)\\
&\quad+\frac{\phi}{\cos\alpha}\frac{1-\nu}{2}\left(n_x^2-n_y^2\right)\left(\mathbf{e}_1^{\mathrm{T}}\otimes\mathbf{D}^{(1)}\right)\\
\mathbf{B}_{22} &= \left[-\tan\alpha(1-\nu)n_x n_y+\frac{1-\nu}{2}\left(n_x^2-n_y^2\right)\right]\left(\mathbf{e}_1^{\mathrm{T}}\mathbf{D}^{(1)}\otimes\mathbf{I}\right)\\
&\quad+\frac{\phi}{\cos\alpha}(1-\nu)n_x n_y\left(\mathbf{e}_1^{\mathrm{T}}\otimes\mathbf{D}^{(1)}\right)
\end{aligned}
\tag{37}
$$

- edge DA, SS1

$$
\begin{aligned}
\mathbf{B}_{11} &= n_y\left(\mathbf{e}_1^{\mathrm{T}}\otimes\mathbf{I}\right)\\
\mathbf{B}_{12} &= -n_x\left(\mathbf{e}_1^{\mathrm{T}}\otimes\mathbf{I}\right)\\
\mathbf{B}_{21} &= \left[\left(n_x^2+\nu n_y^2\right)-(1-\nu)\tan\alpha\, n_x n_y\right]\left(\mathbf{e}_1^{\mathrm{T}}\mathbf{D}^{(1)}\otimes\mathbf{I}\right)\\
&\quad+\frac{\phi}{\cos\alpha}(1-\nu)n_x n_y\left(\mathbf{e}_1^{\mathrm{T}}\otimes\mathbf{D}^{(1)}\right)\\
\mathbf{B}_{22} &= \left[-\tan\alpha\left(\nu n_x^2+n_y^2\right)+(1-\nu)n_x n_y\right]\left(\mathbf{e}_1^{\mathrm{T}}\mathbf{D}^{(1)}\otimes\mathbf{I}\right)\\
&\quad+\frac{\phi}{\cos\alpha}\left(\nu n_x^2+n_y^2\right)\left(\mathbf{e}_1^{\mathrm{T}}\otimes\mathbf{D}^{(1)}\right)
\end{aligned}
\tag{38}
$$

- edge DA, SS2

$$
\begin{aligned}
\mathbf{B}_{11} &= n_x\left(\mathbf{e}_1^{\mathrm{T}}\otimes\mathbf{I}\right)\\
\mathbf{B}_{12} &= n_y\left(\mathbf{e}_1^{\mathrm{T}}\otimes\mathbf{I}\right)\\
\mathbf{B}_{21} &= \left[(\nu-1)n_x n_y-\tan\alpha\frac{1-\nu}{2}\left(n_x^2-n_y^2\right)\right]\left(\mathbf{e}_1^{\mathrm{T}}\mathbf{D}^{(1)}\otimes\mathbf{I}\right)\\
&\quad+\frac{\phi}{\cos\alpha}\frac{1-\nu}{2}\left(n_x^2-n_y^2\right)\left(\mathbf{e}_1^{\mathrm{T}}\otimes\mathbf{D}^{(1)}\right)\\
\mathbf{B}_{22} &= \left[-\tan\alpha(1-\nu)n_x n_y+\frac{1-\nu}{2}\left(n_x^2-n_y^2\right)\right]\left(\mathbf{e}_1^{\mathrm{T}}\mathbf{D}^{(1)}\otimes\mathbf{I}\right)\\
&\quad+\frac{\phi}{\cos\alpha}(1-\nu)n_x n_y\left(\mathbf{e}_1^{\mathrm{T}}\otimes\mathbf{D}^{(1)}\right)
\end{aligned}
\tag{39}
$$

- edge AB, clamped

$$
\begin{aligned}
\mathbf{B}_{11} &= n_x \left(\mathbf{I} \otimes \mathbf{e}_1^{\mathrm{T}}\right) \\
\mathbf{B}_{12} &= n_y \left(\mathbf{I} \otimes \mathbf{e}_1^{\mathrm{T}}\right) \\
\mathbf{B}_{21} &= n_y \left(\mathbf{I} \otimes \mathbf{e}_1^{\mathrm{T}}\right) \\
\mathbf{B}_{22} &= -n_x \left(\mathbf{I} \otimes \mathbf{e}_1^{\mathrm{T}}\right)
\end{aligned}
\tag{40}
$$

- edge AB, free

$$
\begin{aligned}
\mathbf{B}_{11} &= \left[\left(n_x^2 + \nu n_y^2\right) - (1-\nu)\tan\alpha\, n_x n_y\right] \left(\mathbf{D}^{(1)} \otimes \mathbf{e}_1^{\mathrm{T}}\right) \\
&\quad + \frac{\phi}{\cos\alpha}(1-\nu) n_x n_y \left(\mathbf{I} \otimes \mathbf{e}_1^{\mathrm{T}} \mathbf{D}^{(1)}\right) \\
\mathbf{B}_{12} &= \left[-\tan\alpha\left(\nu n_x^2 + n_y^2\right) + (1-\nu) n_x n_y\right] \left(\mathbf{D}^{(1)} \otimes \mathbf{e}_1^{\mathrm{T}}\right) \\
&\quad + \frac{\phi}{\cos\alpha}\left(\nu n_x^2 + n_y^2\right) \left(\mathbf{I} \otimes \mathbf{e}_1^{\mathrm{T}} \mathbf{D}^{(1)}\right) \\
\mathbf{B}_{21} &= \left[(\nu-1) n_x n_y - \tan\alpha \frac{1-\nu}{2}\left(n_x^2 - n_y^2\right)\right] \left(\mathbf{D}^{(1)} \otimes \mathbf{e}_1^{\mathrm{T}}\right) \\
&\quad + \frac{\phi}{\cos\alpha}\frac{1-\nu}{2}\left(n_x^2 - n_y^2\right) \left(\mathbf{I} \otimes \mathbf{e}_1^{\mathrm{T}} \mathbf{D}^{(1)}\right) \\
\mathbf{B}_{22} &= \left[-\tan\alpha(1-\nu) n_x n_y + \frac{1-\nu}{2}\left(n_x^2 - n_y^2\right)\right] \left(\mathbf{D}^{(1)} \otimes \mathbf{e}_1^{\mathrm{T}}\right) \\
&\quad + \frac{\phi}{\cos\alpha}(1-\nu) n_x n_y \left(\mathbf{I} \otimes \mathbf{e}_1^{\mathrm{T}} \mathbf{D}^{(1)}\right)
\end{aligned}
\tag{41}
$$

- edge AB, SS1

$$
\begin{aligned}
\mathbf{B}_{11} &= n_y \left(\mathbf{I} \otimes \mathbf{e}_1^{\mathrm{T}}\right) \\
\mathbf{B}_{12} &= -n_x \left(\mathbf{I} \otimes \mathbf{e}_1^{\mathrm{T}}\right) \\
\mathbf{B}_{21} &= \left[\left(n_x^2 + \nu n_y^2\right) - (1-\nu)\tan\alpha\, n_x n_y\right] \left(\mathbf{D}^{(1)} \otimes \mathbf{e}_1^{\mathrm{T}}\right) \\
&\quad + \frac{\phi}{\cos\alpha}(1-\nu) n_x n_y \left(\mathbf{I} \otimes \mathbf{e}_1^{\mathrm{T}} \mathbf{D}^{(1)}\right) \\
\mathbf{B}_{22} &= \left[-\tan\alpha\left(\nu n_x^2 + n_y^2\right) + (1-\nu) n_x n_y\right] \left(\mathbf{D}^{(1)} \otimes \mathbf{e}_1^{\mathrm{T}}\right) \\
&\quad + \frac{\phi}{\cos\alpha}\left(\nu n_x^2 + n_y^2\right) \left(\mathbf{I} \otimes \mathbf{e}_1^{\mathrm{T}} \mathbf{D}^{(1)}\right)
\end{aligned}
\tag{42}
$$

- edge AB, SS2

$$
\begin{aligned}
\mathbf{B}_{11} &= n_x \left(\mathbf{I} \otimes \mathbf{e}_1^{\mathrm{T}}\right) \\
\mathbf{B}_{12} &= n_y \left(\mathbf{I} \otimes \mathbf{e}_1^{\mathrm{T}}\right) \\
\mathbf{B}_{21} &= \left[(\nu-1)n_x n_y - \tan\alpha \frac{1-\nu}{2}\left(n_x^2 - n_y^2\right)\right]\left(\mathbf{D}^{(1)} \otimes \mathbf{e}_1^{\mathrm{T}}\right) \\
&\quad + \frac{\phi}{\cos\alpha}\frac{1-\nu}{2}\left(n_x^2 - n_y^2\right)\left(\mathbf{I} \otimes \mathbf{e}_1^{\mathrm{T}}\mathbf{D}^{(1)}\right) \\
\mathbf{B}_{22} &= \left[-\tan\alpha(1-\nu)n_x n_y + \frac{1-\nu}{2}\left(n_x^2 - n_y^2\right)\right]\left(\mathbf{D}^{(1)} \otimes \mathbf{e}_1^{\mathrm{T}}\right) \\
&\quad + \frac{\phi}{\cos\alpha}(1-\nu)n_x n_y \left(\mathbf{I} \otimes \mathbf{e}_1^{\mathrm{T}}\mathbf{D}^{(1)}\right)
\end{aligned}
\tag{43}
$$

- edge BC, clamped

$$
\begin{aligned}
\mathbf{B}_{11} &= n_x \left(\mathbf{e}_{N+1}^{\mathrm{T}} \otimes \mathbf{I}\right) \\
\mathbf{B}_{12} &= n_y \left(\mathbf{e}_{N+1}^{\mathrm{T}} \otimes \mathbf{I}\right) \\
\mathbf{B}_{21} &= n_y \left(\mathbf{e}_{N+1}^{\mathrm{T}} \otimes \mathbf{I}\right) \\
\mathbf{B}_{22} &= -n_x \left(\mathbf{e}_{N+1}^{\mathrm{T}} \otimes \mathbf{I}\right)
\end{aligned}
\tag{44}
$$

- edge BC, free

$$
\begin{aligned}
\mathbf{B}_{11} &= \left[\left(n_x^2 + \nu n_y^2\right) - (1-\nu)\tan\alpha\, n_x n_y\right]\left(\mathbf{e}_{N+1}^{\mathrm{T}}\mathbf{D}^{(1)} \otimes \mathbf{I}\right) \\
&\quad + \frac{\phi}{\cos\alpha}(1-\nu)n_x n_y \left(\mathbf{e}_{N+1}^{\mathrm{T}} \otimes \mathbf{D}^{(1)}\right) \\
\mathbf{B}_{12} &= \left[-\tan\alpha\left(\nu n_x^2 + n_y^2\right) + (1-\nu)n_x n_y\right]\left(\mathbf{e}_{N+1}^{\mathrm{T}}\mathbf{D}^{(1)} \otimes \mathbf{I}\right) \\
&\quad + \frac{\phi}{\cos\alpha}\left(\nu n_x^2 + n_y^2\right)\left(\mathbf{e}_{N+1}^{\mathrm{T}} \otimes \mathbf{D}^{(1)}\right) \\
\mathbf{B}_{21} &= \left[(\nu-1)n_x n_y - \tan\alpha \frac{1-\nu}{2}\left(n_x^2 - n_y^2\right)\right]\left(\mathbf{e}_{N+1}^{\mathrm{T}}\mathbf{D}^{(1)} \otimes \mathbf{I}\right) \\
&\quad + \frac{\phi}{\cos\alpha}\frac{1-\nu}{2}\left(n_x^2 - n_y^2\right)\left(\mathbf{e}_{N+1}^{\mathrm{T}} \otimes \mathbf{D}^{(1)}\right) \\
\mathbf{B}_{22} &= \left[-\tan\alpha(1-\nu)n_x n_y + \frac{1-\nu}{2}\left(n_x^2 - n_y^2\right)\right]\left(\mathbf{e}_{N+1}^{\mathrm{T}}\mathbf{D}^{(1)} \otimes \mathbf{I}\right) \\
&\quad + \frac{\phi}{\cos\alpha}(1-\nu)n_x n_y \left(\mathbf{e}_{N+1}^{\mathrm{T}} \otimes \mathbf{D}^{(1)}\right)
\end{aligned}
\tag{45}
$$

- edge BC, SS1

$$
\begin{aligned}
\mathbf{B}_{11} &= n_y \left(\mathbf{e}_{N+1}^{\mathrm{T}} \otimes \mathbf{I}\right) \\
\mathbf{B}_{12} &= -n_x \left(\mathbf{e}_{N+1}^{\mathrm{T}} \otimes \mathbf{I}\right) \\
\mathbf{B}_{21} &= \left[\left(n_x^2 + \nu n_y^2\right) - (1-\nu)\tan\alpha\, n_x n_y\right] \left(\mathbf{e}_{N+1}^{\mathrm{T}} \mathbf{D}^{(1)} \otimes \mathbf{I}\right) \\
&\quad + \frac{\phi}{\cos\alpha}(1-\nu) n_x n_y \left(\mathbf{e}_{N+1}^{\mathrm{T}} \otimes \mathbf{D}^{(1)}\right) \\
\mathbf{B}_{22} &= \left[-\tan\alpha\left(\nu n_x^2 + n_y^2\right) + (1-\nu) n_x n_y\right] \left(\mathbf{e}_{N+1}^{\mathrm{T}} \mathbf{D}^{(1)} \otimes \mathbf{I}\right) \\
&\quad + \frac{\phi}{\cos\alpha}\left(\nu n_x^2 + n_y^2\right) \left(\mathbf{e}_{N+1}^{\mathrm{T}} \otimes \mathbf{D}^{(1)}\right)
\end{aligned}
\tag{46}
$$

- edge BC, SS2

$$
\begin{aligned}
\mathbf{B}_{11} &= n_x \left(\mathbf{e}_{N+1}^{\mathrm{T}} \otimes \mathbf{I}\right) \\
\mathbf{B}_{12} &= n_y \left(\mathbf{e}_{N+1}^{\mathrm{T}} \otimes \mathbf{I}\right) \\
\mathbf{B}_{21} &= \left[(\nu-1) n_x n_y - \tan\alpha \frac{1-\nu}{2}\left(n_x^2 - n_y^2\right)\right] \left(\mathbf{e}_{N+1}^{\mathrm{T}} \mathbf{D}^{(1)} \otimes \mathbf{I}\right) \\
&\quad + \frac{\phi}{\cos\alpha}\frac{1-\nu}{2}\left(n_x^2 - n_y^2\right) \left(\mathbf{e}_{N+1}^{\mathrm{T}} \otimes \mathbf{D}^{(1)}\right) \\
\mathbf{B}_{22} &= \left[-\tan\alpha(1-\nu) n_x n_y + \frac{1-\nu}{2}\left(n_x^2 - n_y^2\right)\right] \left(\mathbf{e}_{N+1}^{\mathrm{T}} \mathbf{D}^{(1)} \otimes \mathbf{I}\right) \\
&\quad + \frac{\phi}{\cos\alpha}(1-\nu) n_x n_y \left(\mathbf{e}_{N+1}^{\mathrm{T}} \otimes \mathbf{D}^{(1)}\right)
\end{aligned}
\tag{47}
$$

- edge CD, clamped

$$
\begin{aligned}
\mathbf{B}_{11} &= n_x \left(\mathbf{I} \otimes \mathbf{e}_{N+1}^{\mathrm{T}}\right) \\
\mathbf{B}_{12} &= n_y \left(\mathbf{I} \otimes \mathbf{e}_{N+1}^{\mathrm{T}}\right) \\
\mathbf{B}_{21} &= n_y \left(\mathbf{I} \otimes \mathbf{e}_{N+1}^{\mathrm{T}}\right) \\
\mathbf{B}_{22} &= -n_x \left(\mathbf{I} \otimes \mathbf{e}_{N+1}^{\mathrm{T}}\right)
\end{aligned}
\tag{48}
$$

- edge CD, free

$$
\begin{aligned}
\mathbf{B}_{11} &= \left[\left(n_x^2+\nu n_y^2\right)-(1-\nu)\tan\alpha\, n_x n_y\right]\left(\mathbf{D}^{(1)}\otimes\mathbf{e}_{N+1}^{\mathrm{T}}\right)\\
&\quad+\frac{\phi}{\cos\alpha}(1-\nu)n_x n_y\left(\mathbf{I}\otimes\mathbf{e}_{N+1}^{\mathrm{T}}\mathbf{D}^{(1)}\right)\\
\mathbf{B}_{12} &= \left[-\tan\alpha\left(\nu n_x^2+n_y^2\right)+(1-\nu)n_x n_y\right]\left(\mathbf{D}^{(1)}\otimes\mathbf{e}_{N+1}^{\mathrm{T}}\right)\\
&\quad+\frac{\phi}{\cos\alpha}\left(\nu n_x^2+n_y^2\right)\left(\mathbf{I}\otimes\mathbf{e}_{N+1}^{\mathrm{T}}\mathbf{D}^{(1)}\right)\\
\mathbf{B}_{21} &= \left[(\nu-1)n_x n_y-\tan\alpha\frac{1-\nu}{2}\left(n_x^2-n_y^2\right)\right]\left(\mathbf{D}^{(1)}\otimes\mathbf{e}_{N+1}^{\mathrm{T}}\right)\\
&\quad+\frac{\phi}{\cos\alpha}\frac{1-\nu}{2}\left(n_x^2-n_y^2\right)\left(\mathbf{I}\otimes\mathbf{e}_{N+1}^{\mathrm{T}}\mathbf{D}^{(1)}\right)\\
\mathbf{B}_{22} &= \left[-\tan\alpha(1-\nu)n_x n_y+\frac{1-\nu}{2}\left(n_x^2-n_y^2\right)\right]\left(\mathbf{D}^{(1)}\otimes\mathbf{e}_{N+1}^{\mathrm{T}}\right)\\
&\quad+\frac{\phi}{\cos\alpha}(1-\nu)n_x n_y\left(\mathbf{I}\otimes\mathbf{e}_{N+1}^{\mathrm{T}}\mathbf{D}^{(1)}\right)
\end{aligned}
\tag{49}
$$

- edge CD, SS1

$$
\begin{aligned}
\mathbf{B}_{11} &= n_y\left(\mathbf{I}\otimes\mathbf{e}_{N+1}^{\mathrm{T}}\right)\\
\mathbf{B}_{12} &= -n_x\left(\mathbf{I}\otimes\mathbf{e}_{N+1}^{\mathrm{T}}\right)\\
\mathbf{B}_{21} &= \left[\left(n_x^2+\nu n_y^2\right)-(1-\nu)\tan\alpha\, n_x n_y\right]\left(\mathbf{D}^{(1)}\otimes\mathbf{e}_{N+1}^{\mathrm{T}}\right)\\
&\quad+\frac{\phi}{\cos\alpha}(1-\nu)n_x n_y\left(\mathbf{I}\otimes\mathbf{e}_{N+1}^{\mathrm{T}}\mathbf{D}^{(1)}\right)\\
\mathbf{B}_{22} &= \left[-\tan\alpha\left(\nu n_x^2+n_y^2\right)+(1-\nu)n_x n_y\right]\left(\mathbf{D}^{(1)}\otimes\mathbf{e}_{N+1}^{\mathrm{T}}\right)\\
&\quad+\frac{\phi}{\cos\alpha}\left(\nu n_x^2+n_y^2\right)\left(\mathbf{I}\otimes\mathbf{e}_{N+1}^{\mathrm{T}}\mathbf{D}^{(1)}\right)
\end{aligned}
\tag{50}
$$

- edge CD, SS2

$$
\begin{aligned}
\mathbf{B}_{11} &= n_x\left(\mathbf{I}\otimes\mathbf{e}_{N+1}^{\mathrm{T}}\right)\\
\mathbf{B}_{12} &= n_y\left(\mathbf{I}\otimes\mathbf{e}_{N+1}^{\mathrm{T}}\right)\\
\mathbf{B}_{21} &= \left[(\nu-1)n_x n_y-\tan\alpha\frac{1-\nu}{2}\left(n_x^2-n_y^2\right)\right]\left(\mathbf{D}^{(1)}\otimes\mathbf{e}_{N+1}^{\mathrm{T}}\right)\\
&\quad+\frac{\phi}{\cos\alpha}\frac{1-\nu}{2}\left(n_x^2-n_y^2\right)\left(\mathbf{I}\otimes\mathbf{e}_{N+1}^{\mathrm{T}}\mathbf{D}^{(1)}\right)\\
\mathbf{B}_{22} &= \left[-\tan\alpha(1-\nu)n_x n_y+\frac{1-\nu}{2}\left(n_x^2-n_y^2\right)\right]\left(\mathbf{D}^{(1)}\otimes\mathbf{e}_{N+1}^{\mathrm{T}}\right)\\
&\quad+\frac{\phi}{\cos\alpha}(1-\nu)n_x n_y\left(\mathbf{I}\otimes\mathbf{e}_{N+1}^{\mathrm{T}}\mathbf{D}^{(1)}\right)
\end{aligned}
\tag{51}
$$